Electronic Supplementary Material (ESI) for Journal of Materials Chemistry C.

Directing the solid-state photochromic and luminescent behaviors of spiromolecules with Dawson and Anderson polyoxometalate units.

Hachem Dridi,‡[a,b] Amandine Boulmier,‡[a] Patrica Bolle,[c] Anne Dolbecq,[a] Jean-Nöel Rebilly,[b] Frédéric Banse,[b] Laurent Ruhlmann,*[d] Hélène Serier-Brault,[c] Rémi Dessapt,*[c] Pierre Mialane,[a] and Olivier Oms*[a]

[a] Institut Lavoisier de Versailles, UMR 8180, Université Paris-Saclay, Université de Versailles Saint-Quentin, 45 avenue des Etats-Unis, 78035 Versailles Cedex, France. E-mail: olivier.oms@uvsq.fr

[b] Institut de Chimie Moléculaire et des Matériaux d'Orsay, Université Paris Sud, Université Paris-Saclay, F-91405 Orsay, France.

[c] Institut des Matériaux Jean Rouxel, Université de Nantes, CNRS, 2 rue de la Houssinière, BP 32229, 44322 Nantes, France. E-mail: remi.dessapt@cnrs-imn.fr

[d] Laboratoire d'Electrochimie et de Chimie Physique du Corps Solide, Institut de Chimie (UMR 7177 CNRS), Université de Strasbourg, 4 rue Blaise Pascal, 67081 Strasbourg Cedex, France. E-mail: lruhlmann@unistra.fr

Figures and Schemes

Figures S20-S23. *HR-ESI-MS spectrum of* ***(TBA)$_5$[P$_2$W$_{15}$V$_3$-SP]*** *(Zooms)*

Figure S24. *IR spectra of (TBA)$_5$[H$_4$P$_2$W$_{15}$V$_3$O$_{62}$] and* ***(TBA)$_5$[P$_2$W$_{15}$V$_3$-SP]***

Figure S25. *TGA curve of* ***(TBA)$_3$[AlMo$_6$-SP]***

Figure S26. *TGA curve of* ***(TBA)$_3$[AlMo$_6$-SN]***

Figure S27. *TGA curve of* ***(TBA)$_5$[P$_2$W$_{15}$V$_3$-SP]***

Figure S28. *Cyclic voltammograms of* ***SP(OH)$_2$*** *(c = 1 mM) at a glassy carbon electrode (d = 3 mm) vs. SCE in CH$_3$CN with 0.1 M TBAPF$_6$ as the supporting electrolyte. Scan rate: 100 mVs^{-1}.*

Figure S29. *Differential UV-Vis-NIR spectroelectrochemical study of* ***SP(OH)$_2$*** *(c = 1 mM) at ambient temperature upon electrochemical oxidation in CH$_3$CN with 0.1 M TBAPF$_6$ as the supporting electrolyte recorded with an optically transparent thin-layer (0.2 mm) electrochemical (OTTLE) cell equipped with an Au minigrid WE and CaF$_2$ optical windows. A) UV-Vis-NIR spectra recorded during the four successive oxidations of the* ***SP(OH)$_2$*** *(between 0 and +1.4 V). Inset shows the corresponding CV at scan rate of 0.02 V.s$^{–1}$. B) Evolution of the intensity of absorption of the differential UV-vis-NIR spectra of* ***SP(OH)$_2$*** *at 988 nm, 514 nm, 305 nm and 242 nm over four switching cycles upon electrochemical reduction in the potential region of the oxidation step*

Figure S30. *A) Cyclic voltammograms of* ***(TBA)$_3$[AlMo$_6$-SN]*** *(c = 1 mM) at a glassy carbon electrode (d = 3 mm) vs. SCE in CH$_3$CN with 0.1 M TBAPF$_6$ as the supporting electrolyte. Scan rate: 100 mVs^{-1}. B) cyclic voltammograms at different scan rates from 0.100 to 1.000 V s^{-1}.C) plots of I_{pc} vs. $v^{1/2}$ for peaks I, II and II'.*

Scheme S1. *Proposed mechanism explaining the spectroelectrochemical properties of* ***SP(OH)$_2$***.

Figure S31. *Cyclic voltammograms of* ***(TBA)$_5$[P$_2$W$_{15}$V$_3$-SP]*** *(c = 1 mM) at a glassy carbon electrode (d = 3 mm) vs. SCE in CH$_3$CN with 0.1 M TBAPF$_6$ as the supporting electrolyte. Scan rate: 100 mVs^{-1}* **.**

Figure S32. *A) UV-Vis-NIR spectroelectrochemical and B) differential UV-Vis-NIR spectroelectrochemical study of* ***(TBA)$_3$[AlMo$_6$-SP]*** *(c = 1 mM) at ambient temperature upon electrochemical oxidation in CH$_3$CN with 0.1 M TBAPF$_6$ as the supporting electrolyte recorded with an optically transparent thin-layer (0.2 mm) electrochemical (OTTLE) cell equipped with an Pt minigrid WE and CaF$_2$ optical windows. Inset shows the corresponding CV at scan rate of 0.02 V.s$^{–1}$.*

Figure S33. *UV-Vis-NIR spectroelectrochemical study of* ***(TBA)$_3$[AlMo$_6$-SN]*** *(c = 1 mM) at ambient temperature upon electrochemical oxidation in CH$_3$CN with 0.1 M TBAPF$_6$ as the supporting electrolyte recorded with an optically transparent thin-layer (0.2 mm) electrochemical (OTTLE) cell equipped with an Au minigrid WE and CaF$_2$ optical windows. Inset shows the corresponding CV at scan rate of 0.02 V.s$^{–1}$.*

Figure S34. *Differential UV-Vis-NIR spectroelectrochemical study of* ***(TBA)$_3$[AlMo$_6$-SN]*** *(c = 1 mM) at ambient temperature upon electrochemical oxidation in CH$_3$CN with 0.1 M TBAPF$_6$ as the supporting electrolyte recorded with an optically transparent thin-layer (0.2 mm) electrochemical (OTTLE) cell equipped with an Au minigrid WE and CaF$_2$ optical windows. Inset shows the corresponding CV at scan rate of 0.02 V.s$^{–1}$.*

Figure S35. *A) and B) Differential UV-Vis-NIR spectroelectrochemical study of* ***(TBA)$_5$[P$_2$W$_{15}$V$_3$-SP]*** *(c = 1 mM) at ambient temperature upon electrochemical oxidation in CH$_3$CN with 0.1 M TBAPF$_6$ as the supporting electrolyte recorded with an optically transparent thin-layer (0.2* *mm) electrochemical (OTTLE) cell equipped with an Au minigrid WE and CaF_2 optical windows. Inset shows the corresponding CV at scan rate of 0.02 $V.s^{-1}$.*

Figure S36. *Kubelka-Munk transformed reflectivity vs wavelength of (a)* **$(TBA)_3[AlMo_6\text{-}SP]$** *(black line),* ***SPTris*** *(red line), and $(TBA)_3[AlMo_6(OH)_3\{(OCH_2)_3CNH_2\}]$ (blue line), (b)* **$(TBA)_3[AlMo_6\text{-}SN]$** *(black line),* ***SNTris*** *(red line), and $(TBA)_3[AlMo_6(OH)_3\{(OCH_2)_3CNH_2\}]$ (blue line) and (c)* **$(TBA)_5[P_2W_{15}V_3\text{-}SP]$** *(black line),* ***SPTris*** *(red line), and $(TBA)_5[H_4P_2W_{15}V_3O_{62}]$ (blue line). The weak absorptions in the visible in the spectra of* **$(TBA)_3[AlMo_6\text{-}SP]$***,* **$(TBA)_3[AlMo_6\text{-}SN]$** *and* ***SPTris*** *are assignable to a small amount of the open "merocyanine" form which is responsible for the slight color of the powdered samples.*

Figure S37. *UV-vis absorption spectrum in acetonitrile (4.6 × 10^{-5} mol/L) of* **$(TBA)_3[AlMo_6\text{-}SN]$***.*

Figure S38. *Kubelka-Munk transformed reflectivity vs wavelength of $(TBA)_3[AlMo_6(OH)_3\{(OCH_2)_3CNH_2\}]$ (black line), $(TBA)_3[MnMo_6O_{18}\{OCH_2)_3CNH_2\}_2]$ (red line) and $(TBA)_5[H_4P_2W_{15}V_3O_{62}]$ (blue line).*

Figure S39. *Evolution of the photogenerated absorption at room temperature for* **$(TBA)_3[AlMo_6\text{-}SN]$** *(a) under visible light (λ_{irr} = 630 nm) after 0, 0.166, 0.333, 0.5, 1, 2, 3, 5, 7, 10, 20, 30, 40, 60, 90 and 120 min, and (b) in the dark during the thermal fading after 0, 2, 4, 8, 12, 20, 35, 60, 90, 120, 150, 180, 210 and 240 min. Insets: Temporal evolutions of $Abs^{620}(t)$. Black lines show the fits of the $Abs^{620}(t)$ vs t plots according to the rate law $Abs^{620}(t) = (A_0\text{-}A_1\text{-}A_2) + A_1exp(-k^f{}_1t) + A_2exp(-k^f{}_2t)$. Percents of absorption loss after 4 hours are also indicated.*

Figure S40. *Evolution of the photogenerated absorption at room temperature for* **$(TBA)_3[AlMo_6\text{-}SP]$** *(a) under visible light (λ_{irr} = 590 nm) after 0, 0.166, 0.333, 0.5, 1, 2, 3, 5, 7, 10, 15, 20, 30, 40, 60, 90, 120, 150, 180, 210, and 240 min, and (b) in the dark during the thermal fading after 0, 2, 4, 8, 12, 20, 35, 60, 90, 120, 150, 180, 210 and 240 min. Inset: Temporal evolutions of $Abs^{570}(t)$. Black lines show the fits of the $Abs^{570}(t)$ vs t plots according to the rate law $Abs^{570}(t) = (A_0\text{-}A_1\text{-}A_2) + A_1exp(-k^f{}_1t) + A_2exp(-k^f{}_2t)$. Percents of absorption loss after 4 hours are also indicated.*

Figure S41. *Evolution of the photogenerated absorption at room temperature for* **$(TBA)_3[MnMo_6\text{-}SP]$** *(a) under visible light (λ_{rr} = 590 nm) after 0, 0.166, 0.333, 0.5, 1, 2, 3, 5, 7, 10, 15, 20, 30, 40, 60, 90, and 120 min, and (b) in the dark during the thermal fading after 0, 2, 4, 8, 12, 20, 35, 60, and 90 min. Inset: Temporal evolutions of $Abs^{580}(t)$. Black lines show the fits of the $Abs^{580}(t)$ vs t plots according to the rate law $Abs^{580}(t) = (A_0\text{-}A_1\text{-}A_2) + A_1exp(-k^f{}_1t) + A_2exp(-k^f{}_2t)$. Percents of absorption loss after 4 hours are also indicated.*

Figure S42. *Evolution of the photogenerated absorption at room temperature under UV irradiation (λ_{irr} = 365 nm) after 0, 0.166, 0.333, 0.5, 1, 2, 3, 4, 5, 6, 10, 20 and 30 min for* **$(TBA)_3[MnMo_6\text{-}SP]$***. Inset: Temporal evolutions of $Abs^{580}(t)$ under 365 nm-UV irradiation. The black line shows the fits of the $Abs^{580}(t)$ vs t plots according to the rate law $Abs^{580}(t) = (A_1 + A_2) - A_1exp(-k^c{}_1t) - A_2exp(-k^c{}_2t)$.*

Figure S43. *Evolution of the maximum of the photogenerated absorption at λ_{max} = 620 nm for* **$(TBA)_3[AlMo_6\text{-}SN]$** *during successive coloration/bleach cycles at room temperature. For one cycle, the sample is exposed to UV light (365 nm) for 20 s, and to red light (630 nm) for 4 min (the black lines display the mean values of the absorption in the coloured and bleached states). After a short period of activation, the hybrid system shows a good cyclability.*

Figure S44. *Kubelka-Munk transformed reflectivity vs wavelength spectra of* **$(TBA)_3[AlMo_6\text{-}SP]$** *before (black solid line) and after 20 min of 365-nm UV irradiation (blue solid line), and* *photoluminescence excitation (PLE) spectrum of **(TBA)$_3$[AlMo$_6$-SP]** monitored at λ_{em} = 675 nm (red dotted line).*

Figure S45. *Evolutions of the merocyanine luminescence (monitored at λ_{exc} = 500 nm) under visible-light irradiation range (λ_{irr} = 590 nm) after 15, 30, 45, and 90 min for **(TBA)$_3$[AlMo$_6$-SP]** (top) and **(TBA)$_3$[MnMo$_6$-SP]** (bottom).*

Thermal behavior

Thermogravimetric analyses (TGA) were done using a Mettler-Toledo TGA apparatus in the temperature range from 25 to 650 °C with a heating rate of 5 $°C \cdot min^{-1}$ and under a flow of oxygen gas at 50 $mL \cdot min^{-1}$.

Electrochemical and Spectroelectrochemical measurements.

Voltammetric data were recorded with a standard three-electrode system using a PARSTAT 2273 potentiostat. The electrolyte was CH_3CN containing 0.1 $mol.L^{-1}$ of tetrabutylammoniumhexafluorophosphate (NBu_4PF_6). Glassy carbon electrode (d = 3 mm) was used as working electrode, and a platinum wire as auxiliary electrode. The reference electrode was the saturated calomel electrode that was electrically connected to the solution by a junction bridge filled with electrolyte.

UV-Vis-NIR spectroelectrochemical experiments were performed with an optically transparent thin-layer electrochemical (OTTLE) cell (University of Reading UK, Hartl, F.) equipped with a Pt grid working electrode and CaF_2 optical windows.[1] UV-Vis-NIR spectroelectrochemical analyses were carried out with a Zeiss MCS 601 UV–Vis–NIR diode array spectrometer. Spectrophotometric analyses of the films were conducted using a 0.1 $mol.L^{-1}$ solution of NBu_4PF_6 in CH_3CN.

[1] M. Krejcik, M. Danek and F. Hartl, *J. Electroanal. Chem.* 1991, ***317***, 179.

Photophysical characterizations

Diffuse reflectance spectra were collected at room temperature on a finely ground sample with a Perkin-Elmer Lambda 1050 spectrometer equipped with a 150 mm diameter integrating sphere coated with Spectralon®, a highly reflecting fluoropolymer. Diffuse reflectance was measured from 250 to 1000 nm with a 2 nm step using Spectralon® as reference (100% reflectance). The reflectance data were treated by a Kubelka-Munk transformation[2] to better determine the absorption thresholds. UV-vis absorption spectra in solution were obtained with the same Perkin-Elmer Lambda 1050 spectrometer. Room-temperature Photoluminescence spectra were recorded on a Jobin-Yvon Fluorolog 3 fluorometer equipped with a photomultiplier (excitation source: 400 W Xe arc lamp and 150W pulsed map for decay times). The emission spectra were corrected for detection and optical spectral response of the spectrofluorimeter and the excitation spectra were weighed for the spectral distribution of the lamp intensity using a photodiode reference detector.

[2] P. Kubelka and F. Munk, *Z. Techn. Physik*, 1931, ***12***, 593.

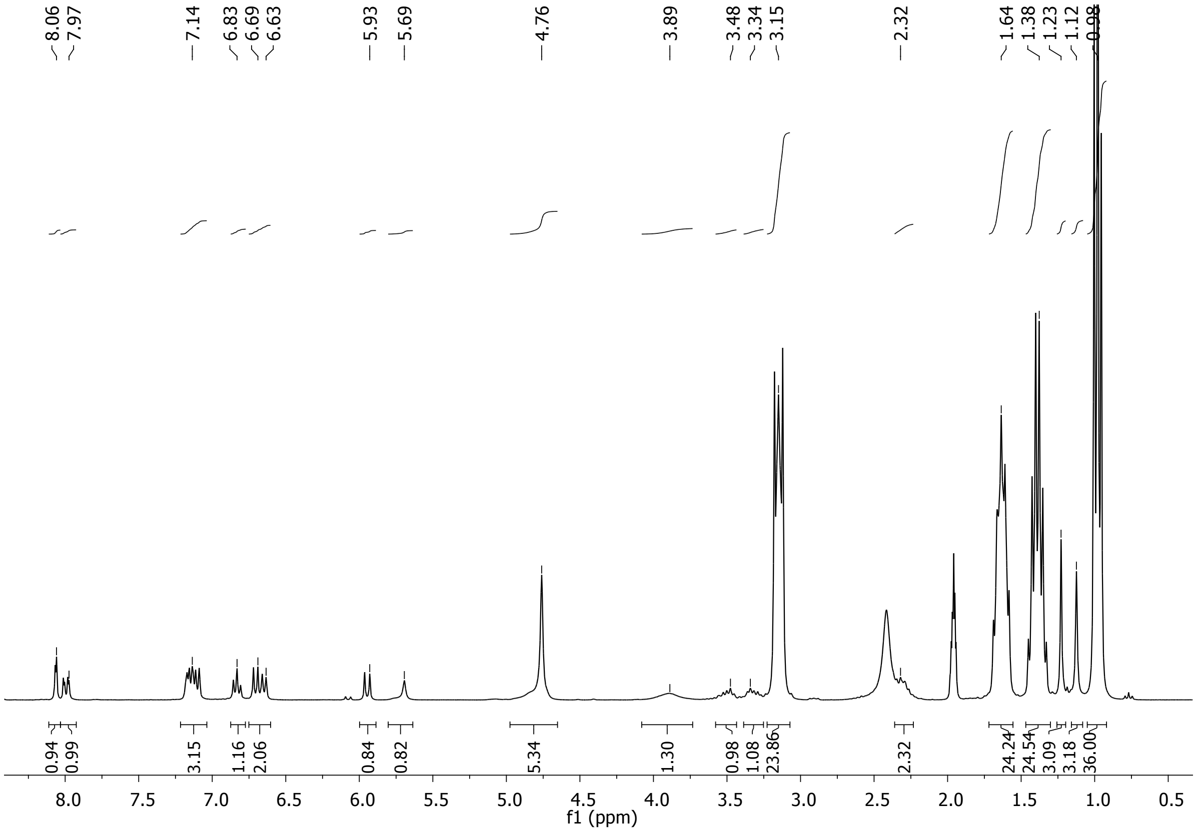

Figure S1 ^{1}H NMR spectrum (CD$_3$CN, 300K, 300 MHz) of **(TBA)$_3$[AlMo$_6$-SP]**

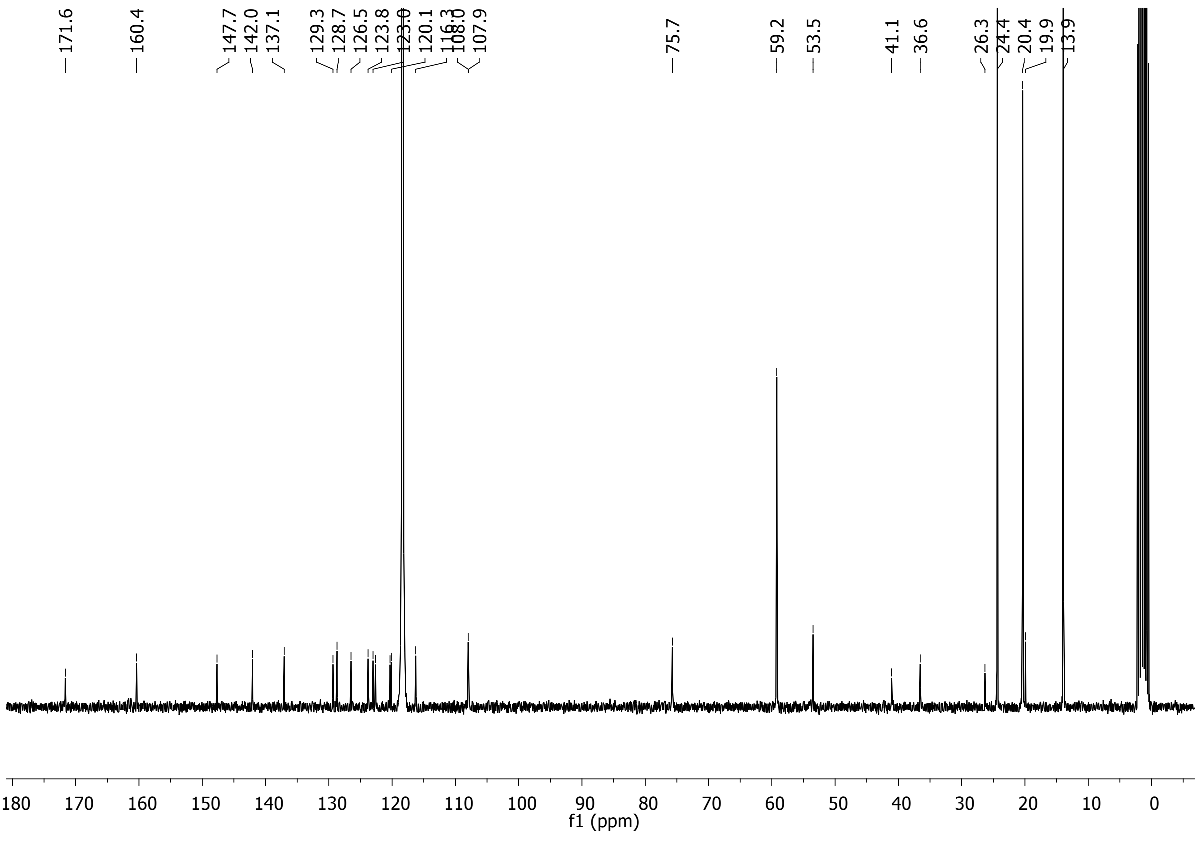

Figure S2 ^{13}C NMR spectrum (CD$_3$CN, 300K, 75 MHz) of **(TBA)$_3$[AlMo$_6$-SP]**

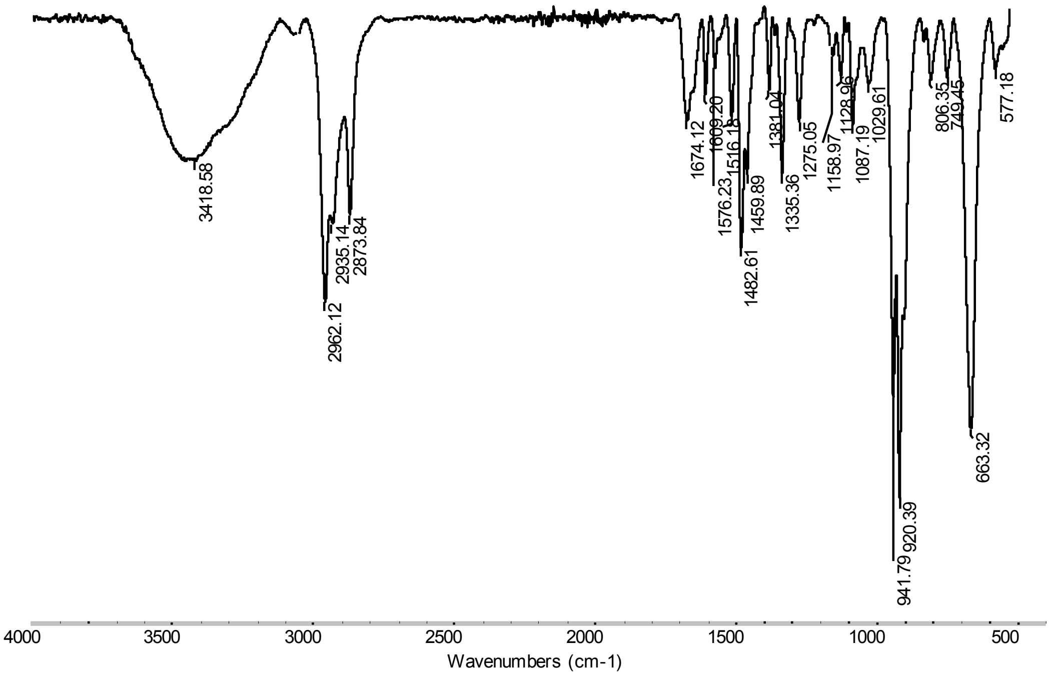

Figure S3 IR-TF spectrum of **$(TBA)_3[AlMo_6$-SP]**

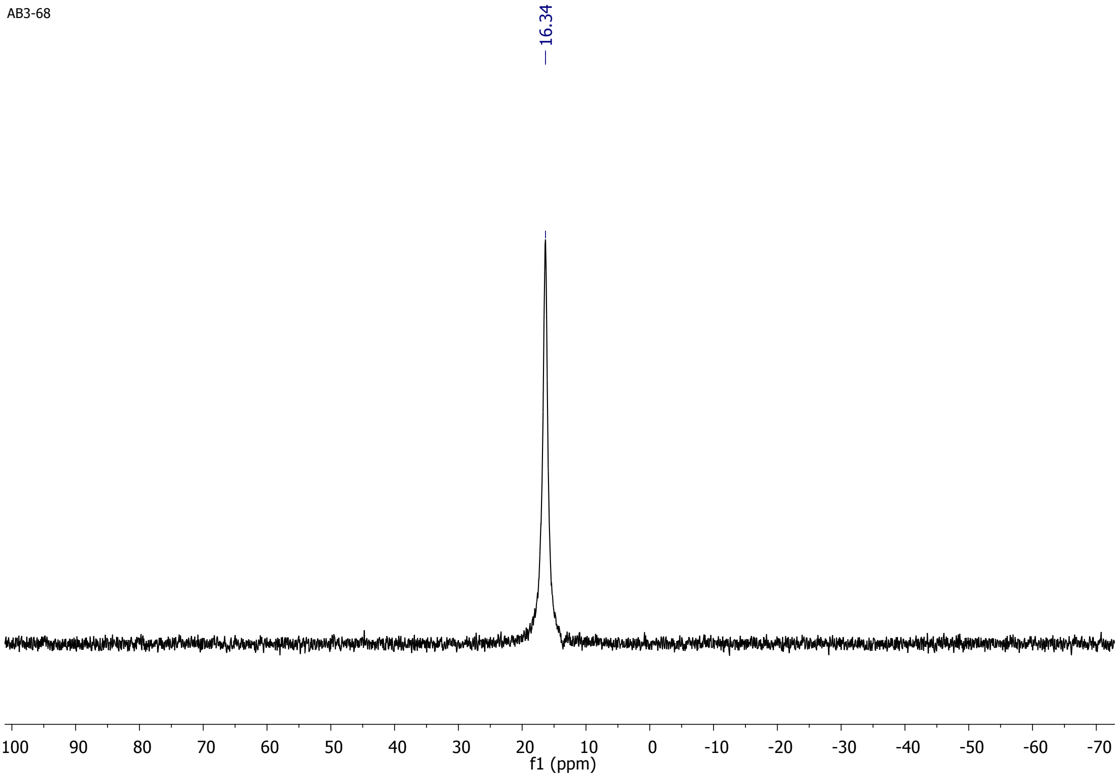

Figure S4 ^{27}Al NMR spectrum (CD_3CN, 300K, 300 MHz) of **$(TBA)_3[AlMo_6$-SP]**

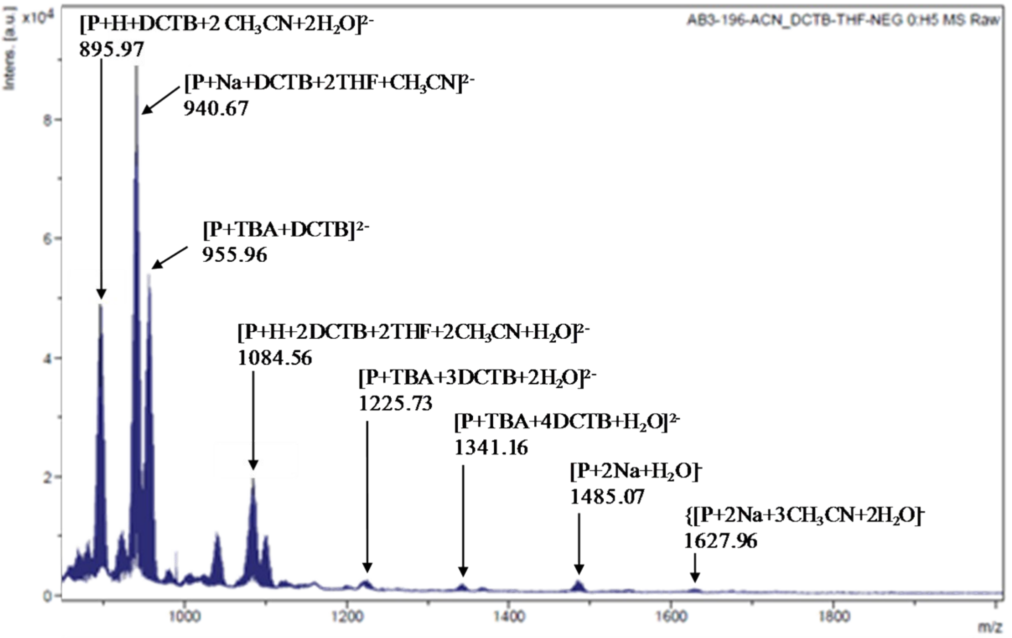

Figure S5 MALDI-TOF mass spectrum of **$(TBA)_3[AlMo_6$-SP]**. P refers to $[AlMo_6\text{-SP}]^{3-}$ and DCTB (*trans*-2-[3-(4-*tert*-Butylphenyl)-2-methyl-2-propenylidene]malononitrile) corresponds to the matrix molecule

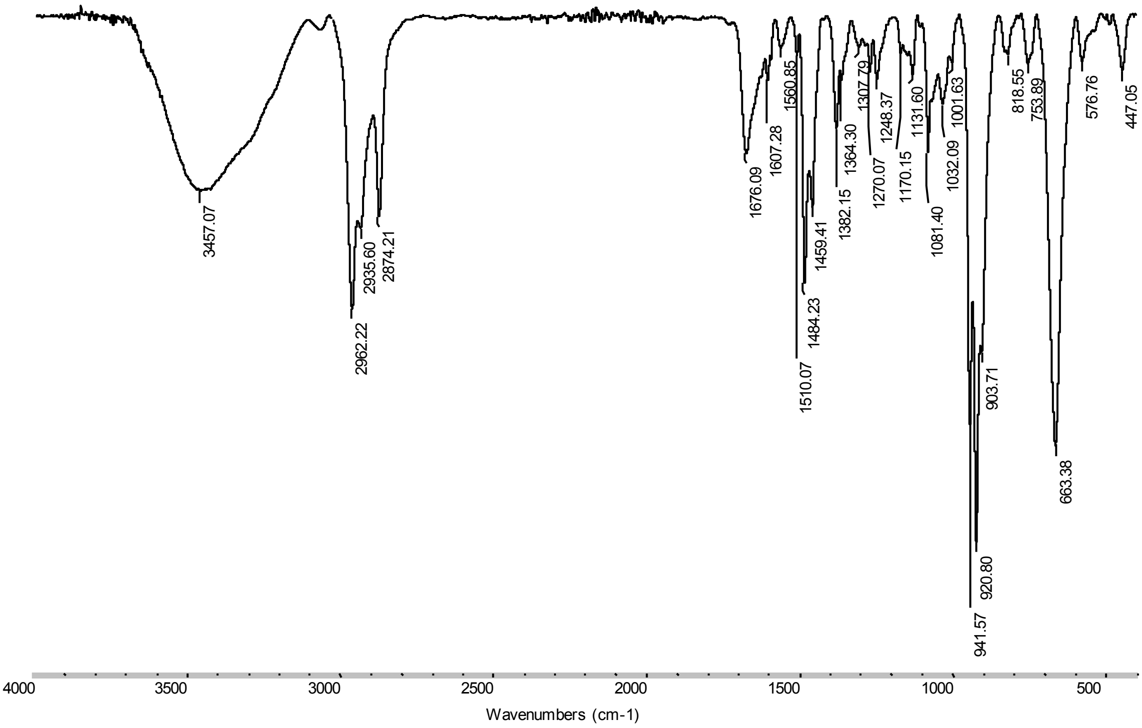

Figure S6 IR-TF spectrum of **$(TBA)_3[AlMo_6$-SN]**

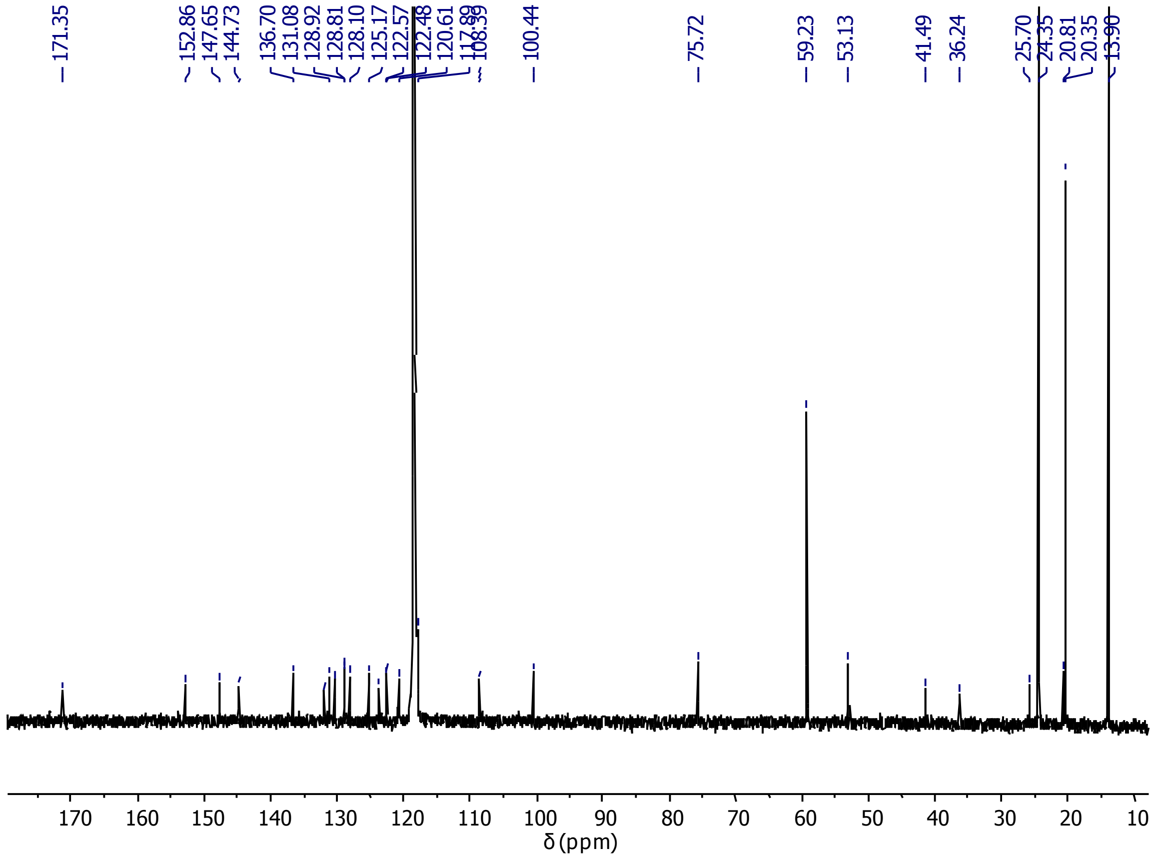

Figure S7 ^{13}C NMR spectrum (CD_3CN, 300K, 75 MHz) of **$(TBA)_3[AlMo_6$-SN]**

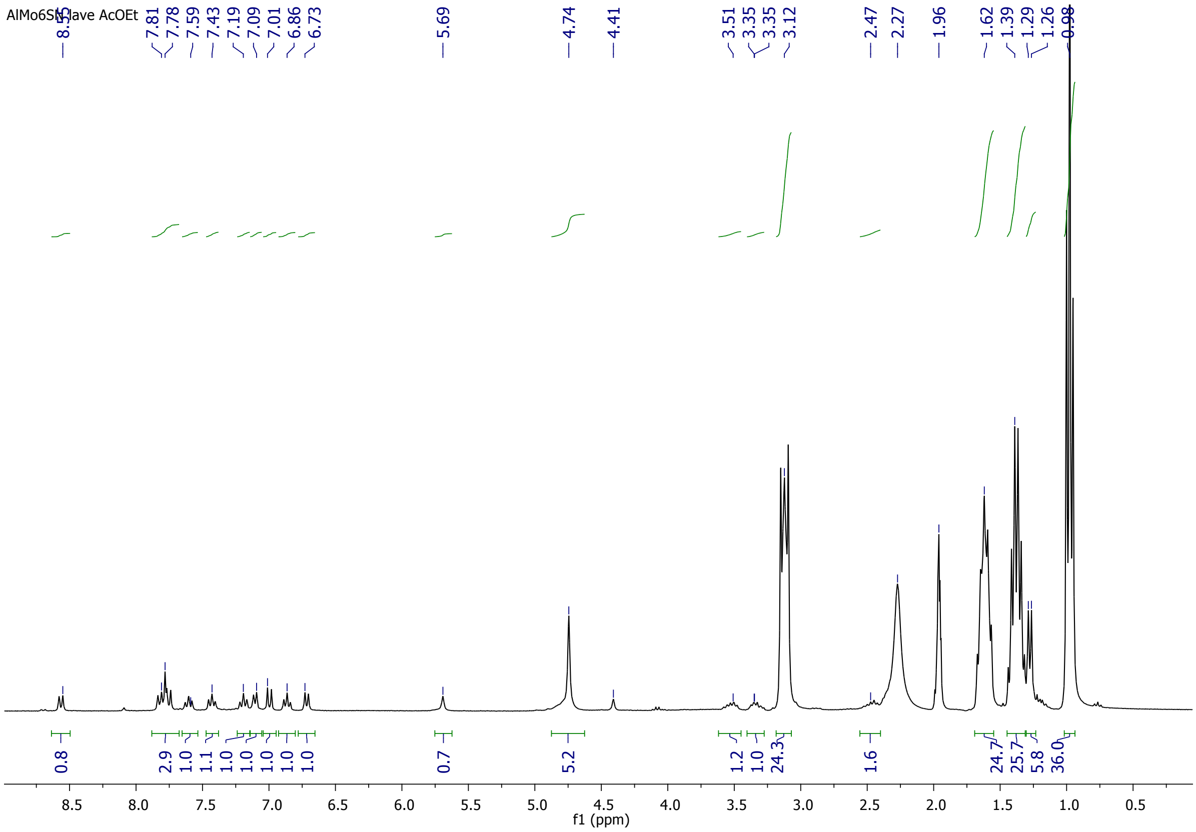

Figure S8 ^{1}H NMR spectrum (CD_3CN, 300K, 300 MHz) of **$(TBA)_3[AlMo_6$-SN]**

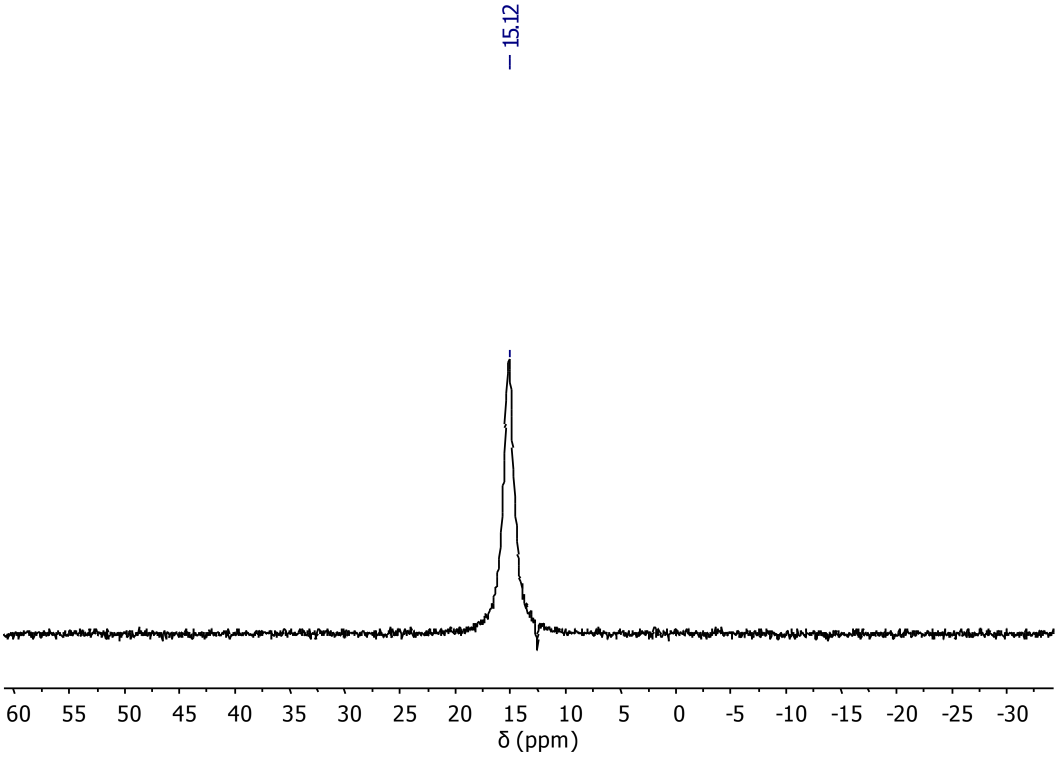

Figure S9 ^{27}Al NMR spectrum (CD_3CN, 300K, 300 MHz) of **$(TBA)_3[AlMo_6$-SN]**

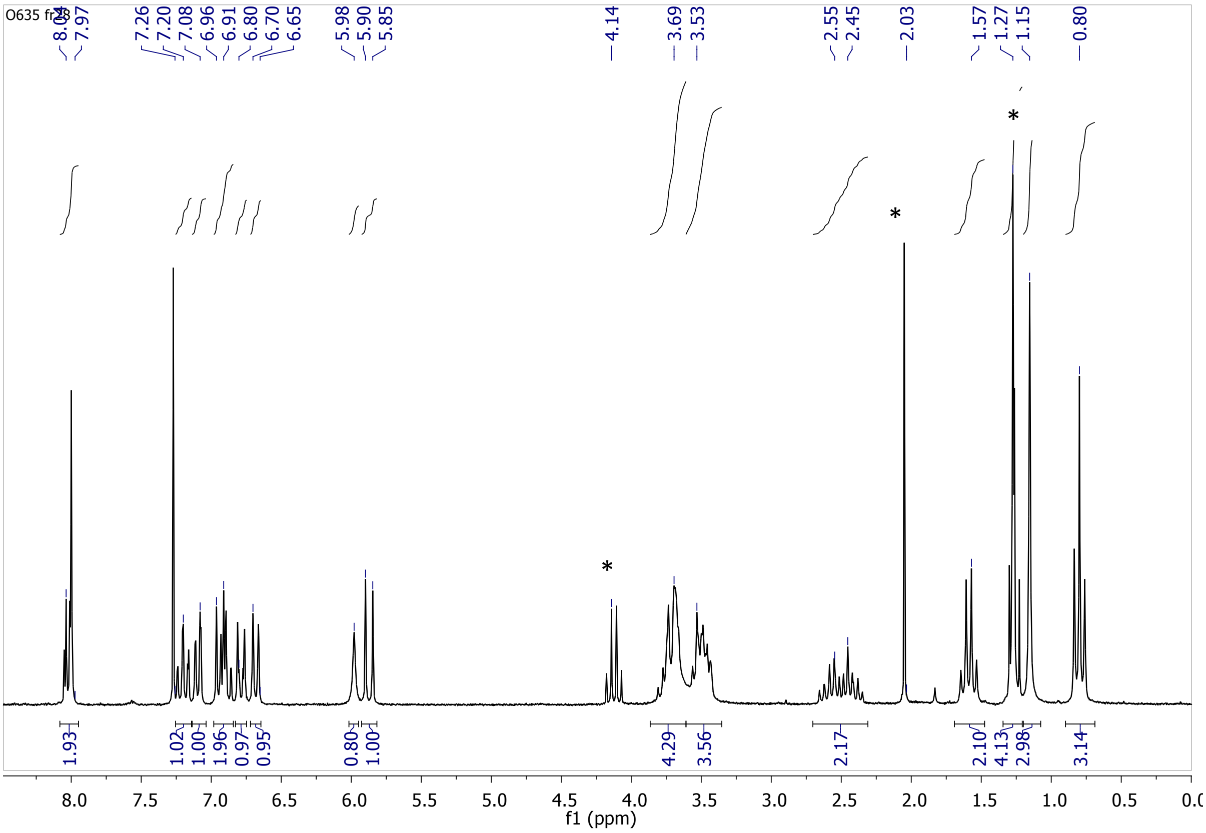

Figure S10 ^{1}H NMR spectrum (CDCl$_3$, 300K, 300 MHz) of **SP(OH)$_2$**. The asterisks indicate the presence of ethyl acetate.

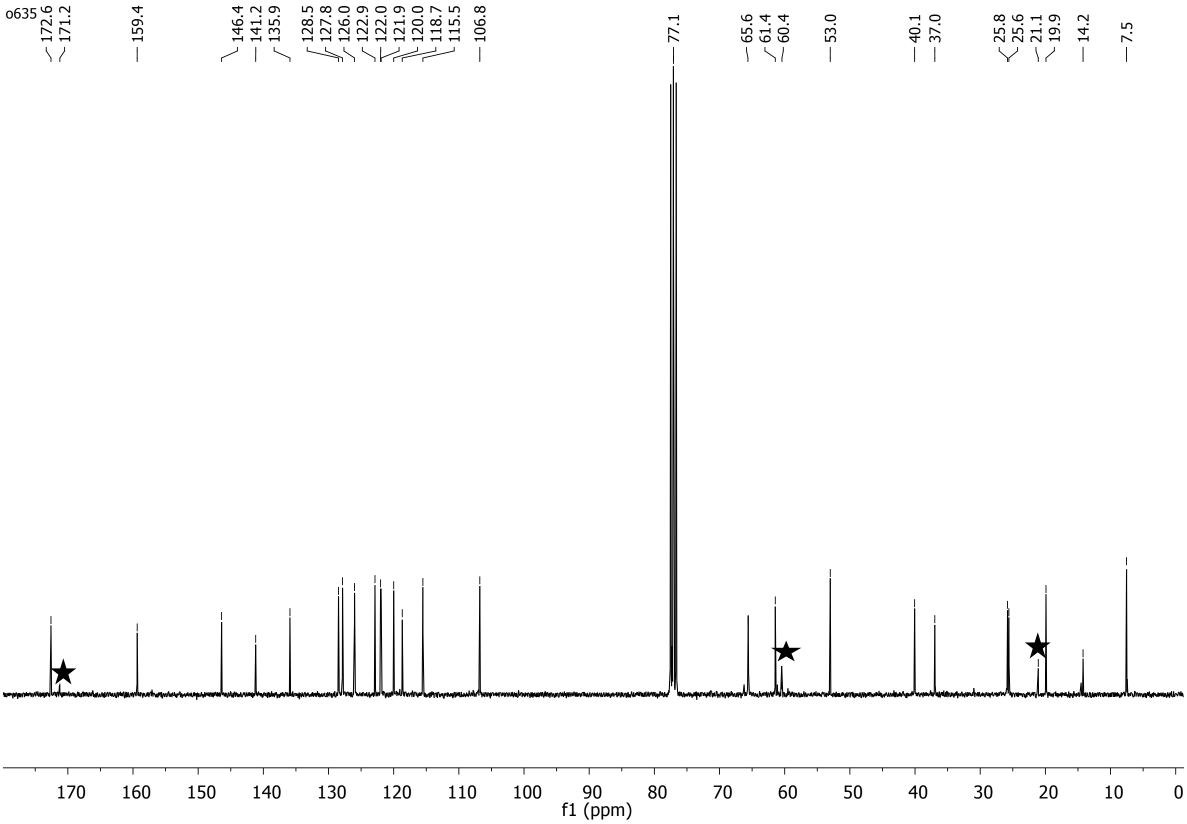

Figure S11 ^{13}C NMR spectrum ($CDCl_3$, 300K, 75 MHz) of **SP(OH)$_2$**. The asterisks indicate the presence of ethyl acetate.

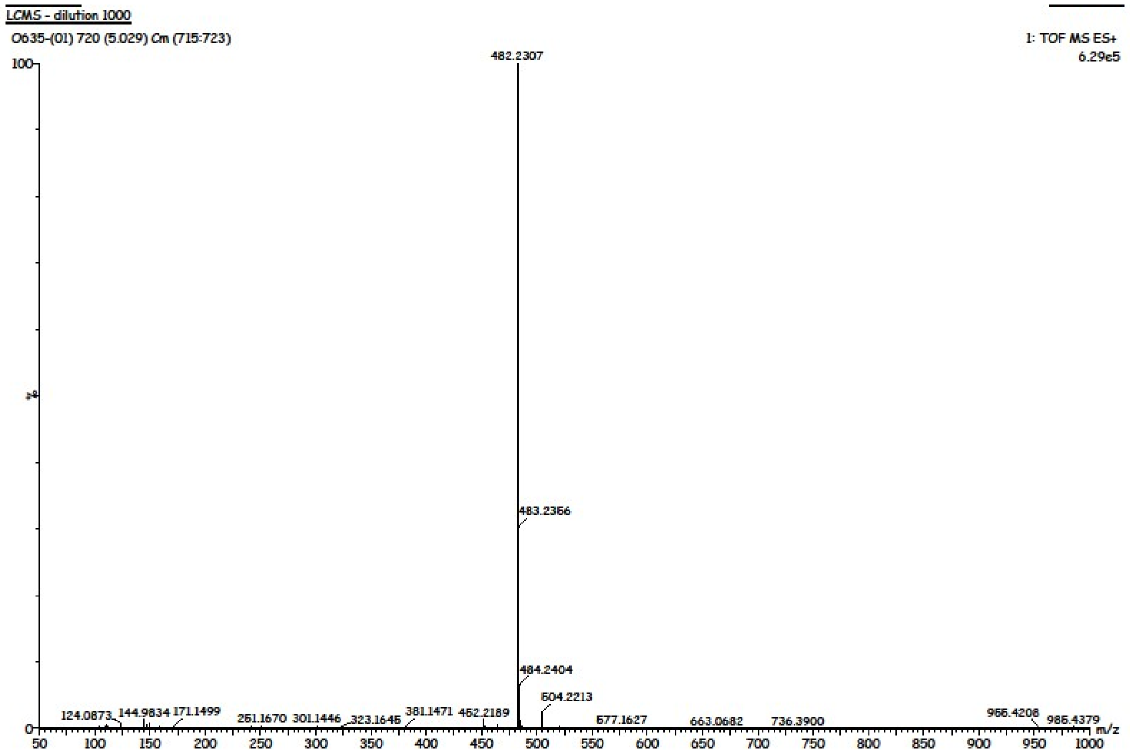

Figure S12 HR-MS of **SP(OH)$_2$**

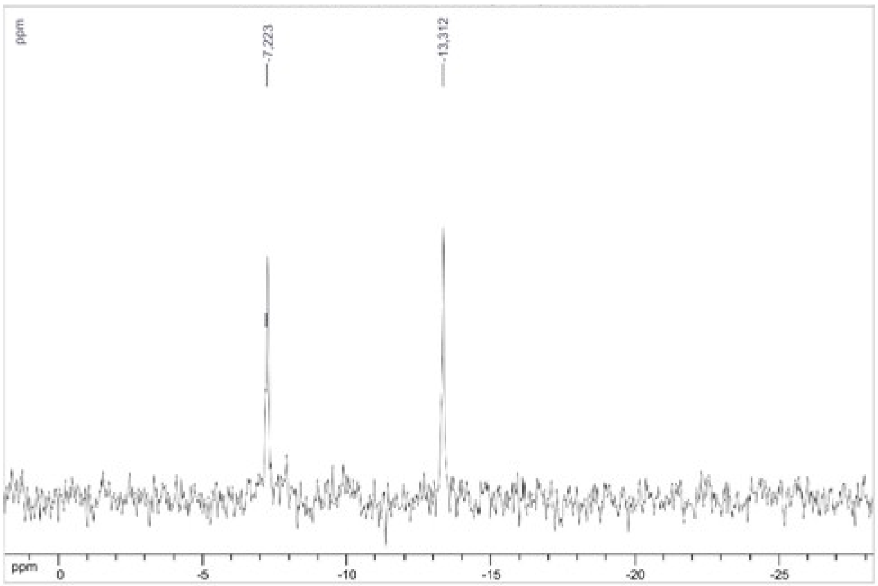

Figure S13 ^{31}P NMR spectrum (CD_3CN, 300K, 250 MHz) of **$(TBA)_5[P_2W_{15}V_3\text{-}SP]$**

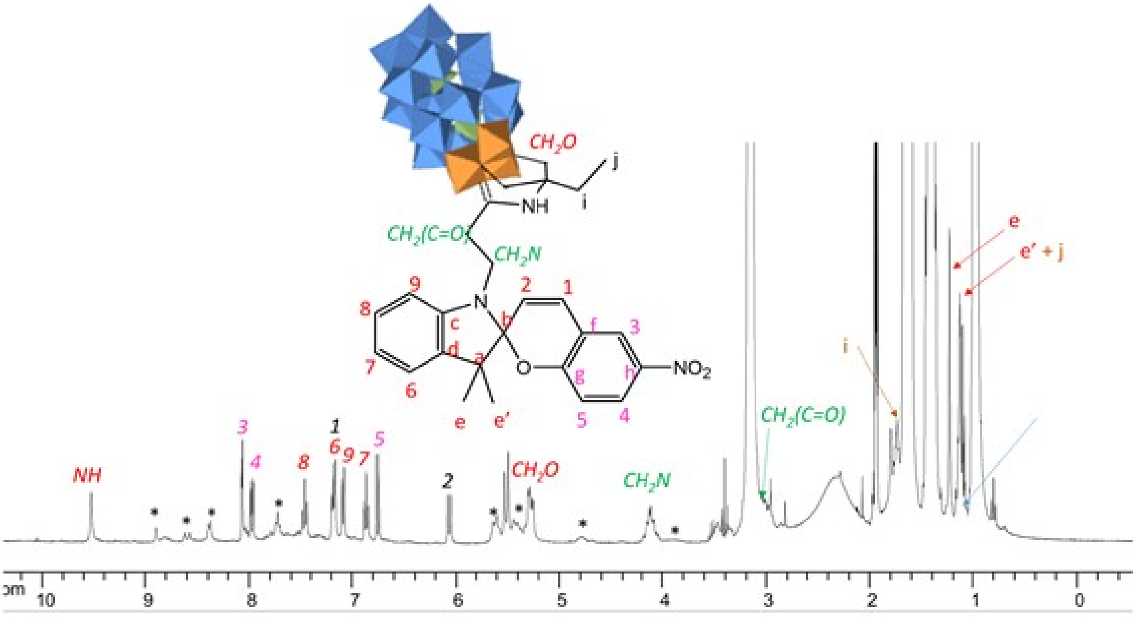

Figure S14 ^{1}H NMR spectrum (CD_3CN, 300K, 360 MHz) of **$(TBA)_5[P_2W_{15}V_3\text{-}SP]$**. The asterisks indicate the resonances of the merocyanine form (open form of the SP).

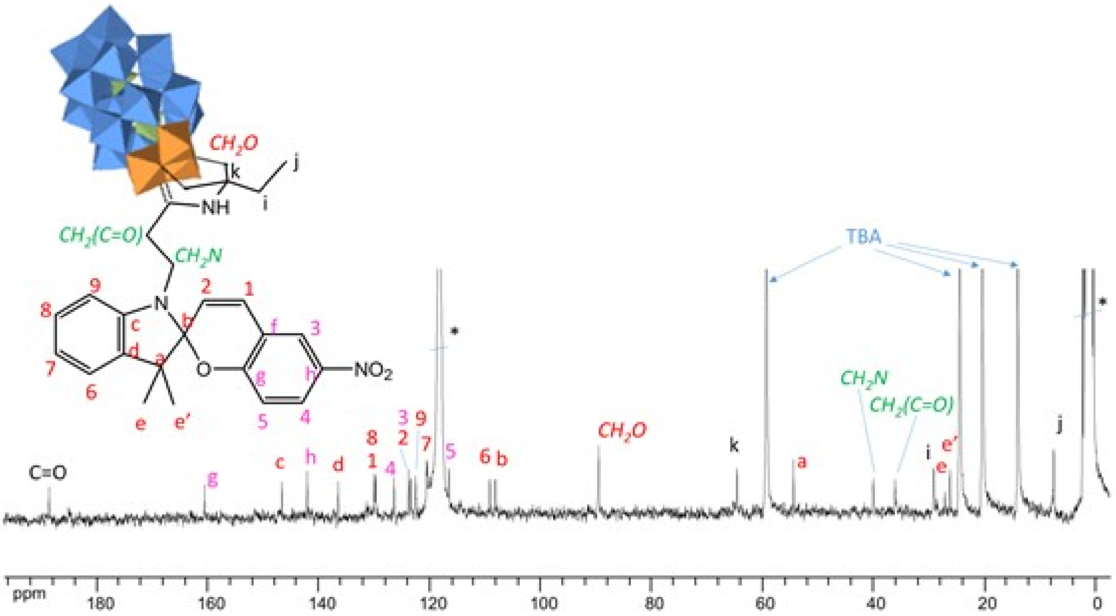

Figure S15 ^{13}C NMR spectrum (CD_3CN, 300K, 62.5 MHz) of **$(TBA)_5[P_2W_{15}V_3\text{-}SP]$**. The asterisks indicate the resonances of the solvent (acetonitrile)

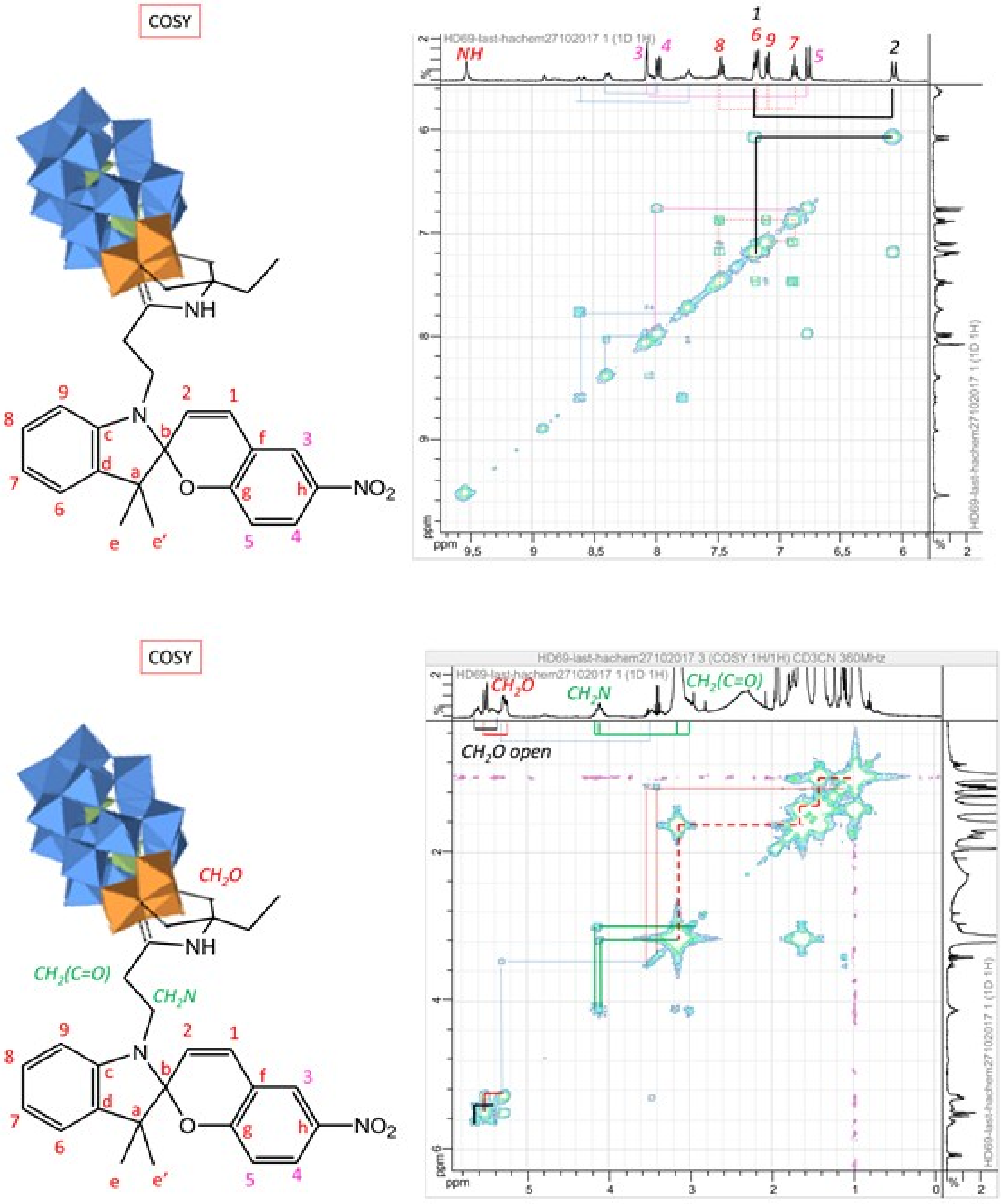

Figure S16 COSY spectrum (CD_3CN, 300K, 360 MHz) of **$(TBA)_5[P_2W_{15}V_3\text{-}SP]$**

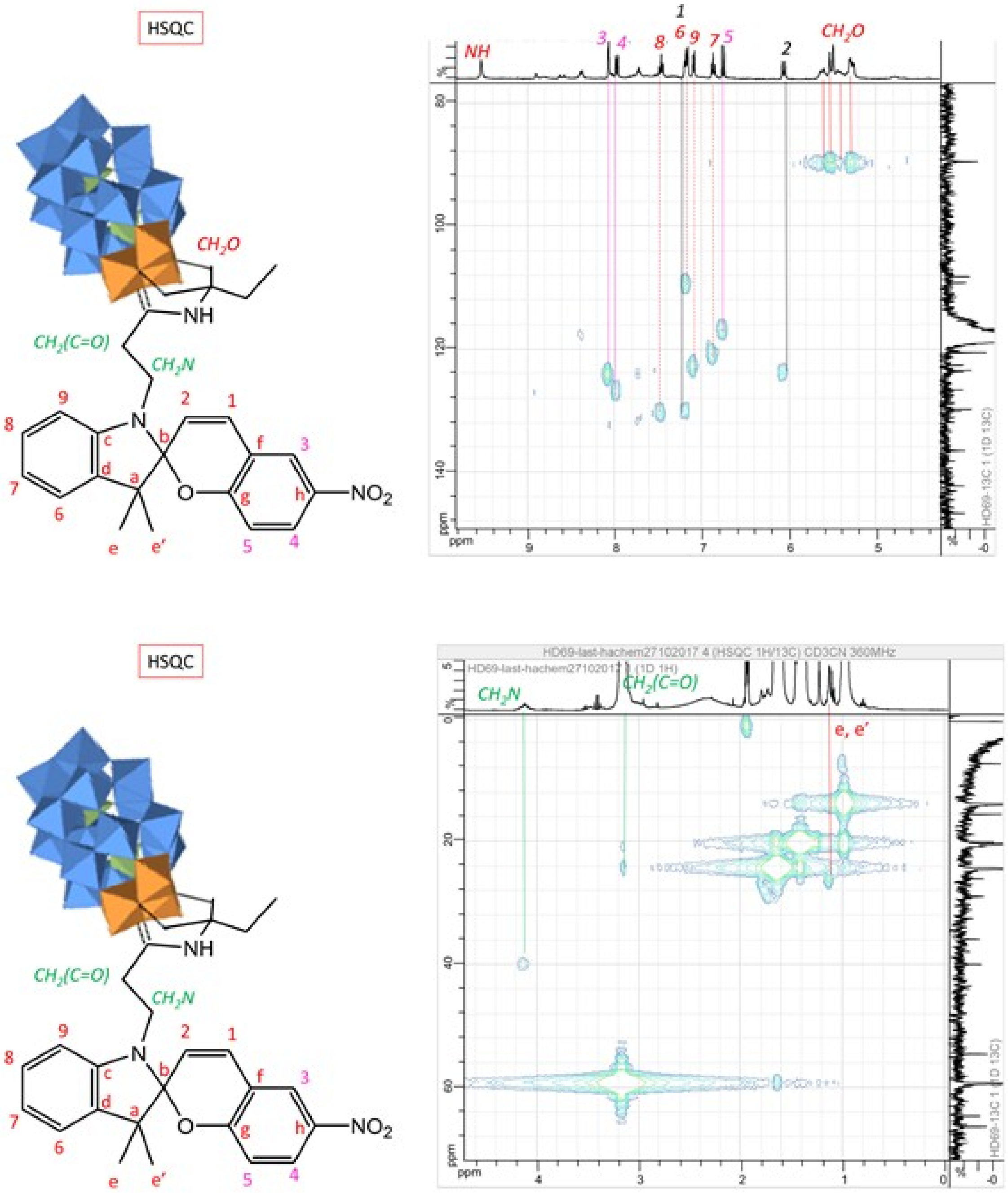

Figure S17 HSQC spectrum (CD_3CN, 300K, 360 MHz) of **$(TBA)_5[P_2W_{15}V_3\text{-}SP]$**

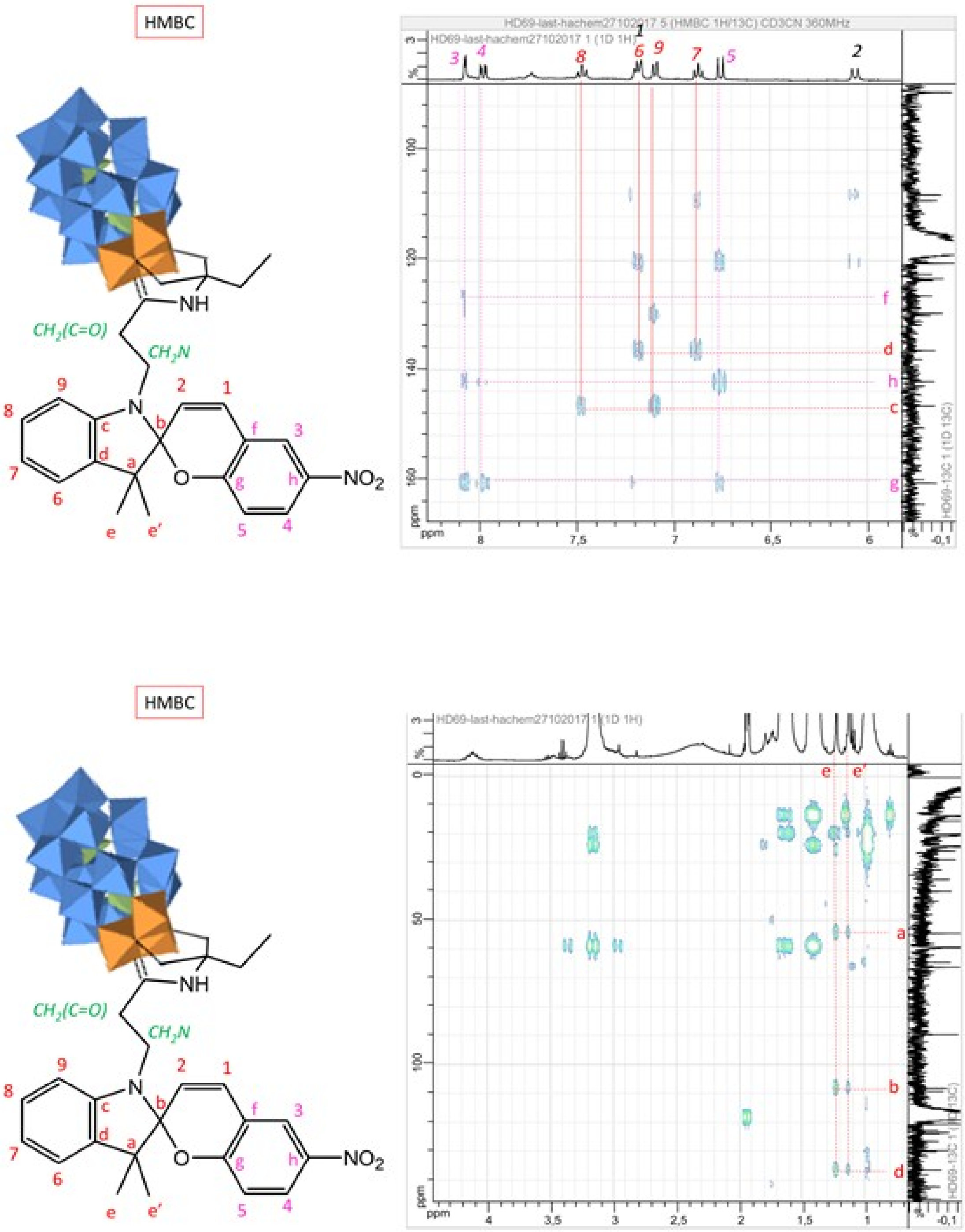

Figure S18 HMBC spectrum (CD_3CN, 300K, 360 MHz) of **$(TBA)_5[P_2W_{15}V_3\text{-}SP]$**

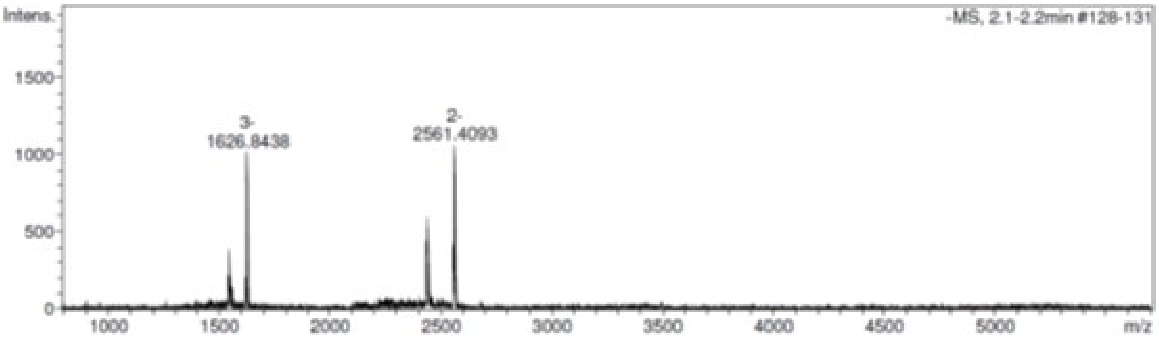

Figure S19 HR-ESI-MS spectrum (negative mode) of **(TBA)$_5$[P$_2$W$_{15}$V$_3$-SP]**

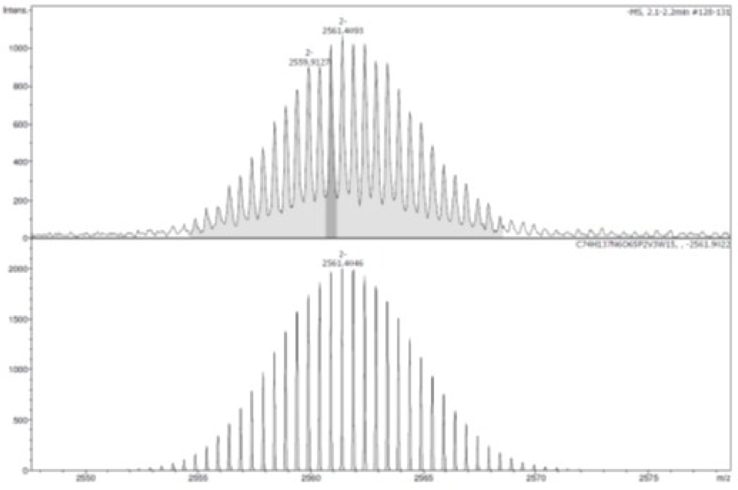

Figure S20 HR-ESI-MS spectrum of **(TBA)$_5$[P$_2$W$_{15}$V$_3$-SP]**
Top: Zoom around the experimental peak at m/z = 2561.4093 (z = -2). *Bottom:* simulated spectrum calcd for formula [M+3TBA]$^{2-}$ with m/z = 2561.4046 (error: 1.8 ppm), M referring to [P$_2$W$_{15}$V$_3$SP]$^{5-}$

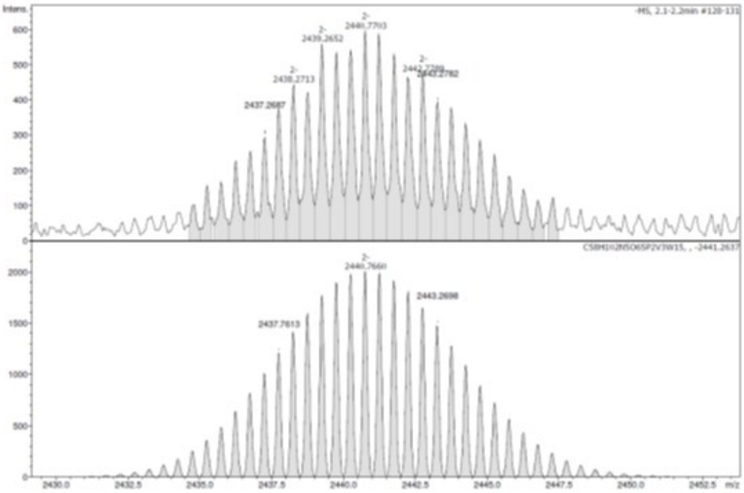

Figure S21 HR-ESI-MS spectrum of **(TBA)$_5$[P$_2$W$_{15}$V$_3$-SP]**
Top: Zoom around the experimental peak at m/z = 2440.7703 (z = -2). *Bottom:* simulated spectrum calcd for formula [M+2TBA+H]$^{2-}$ with m/z = 2440.7660 (error: 1.8 ppm), M referring to [P$_2$W$_{15}$V$_3$SP]$^{5-}$

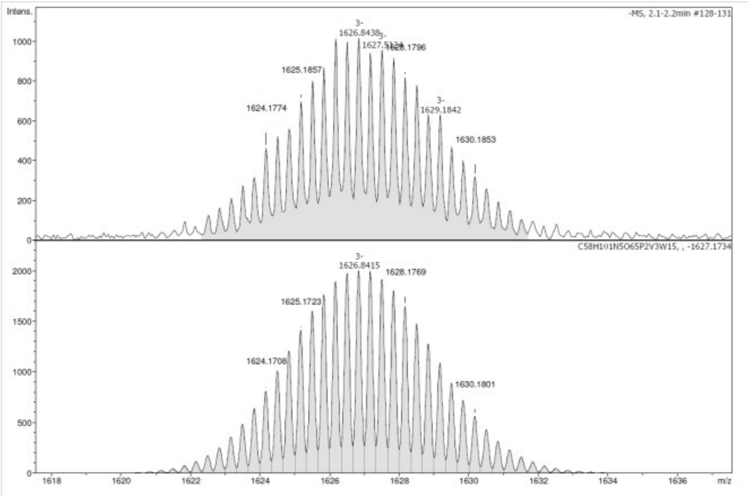

Figure S22 HR-ESI-MS spectrum of **(TBA)$_5$[P$_2$W$_{15}$V$_3$-SP]**.
Top: Zoom around the experimental peak at m/z = 1626.8438 (z = -3). *Bottom:* simulated spectrum calcd for formula [M+2TBA]$^{3-}$ with m/z = 1626.8415 (error: 1.4 ppm), M referring to [P$_2$W$_{15}$V$_3$SP]$^{5-}$

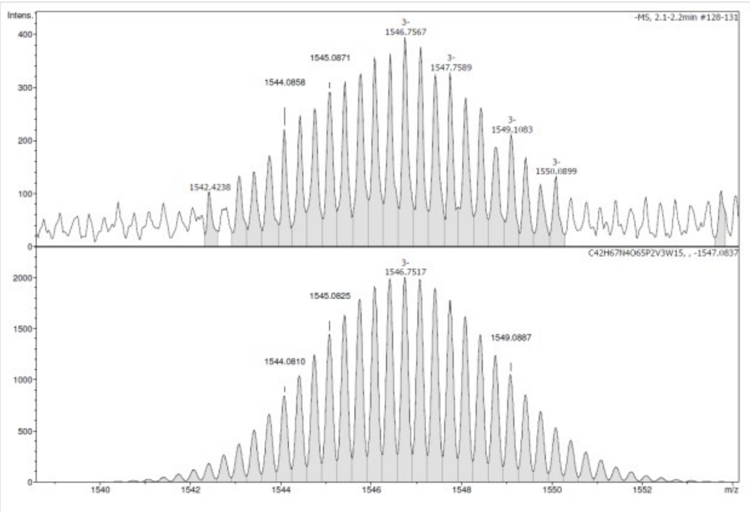

Figure S23 HR-ESI-MS spectrum of **(TBA)$_5$[P$_2$W$_{15}$V$_3$-SP]**.
Top: Zoom around the experimental peak at m/z = 1546.7567 (z = -3). *Bottom:* simulated spectrum calcd for formula [M+TBA+H]$^{3-}$ with m/z = 15467517 (error: 3.2 ppm), M referring to [P$_2$W$_{15}$V$_3$SP]$^{5-}$

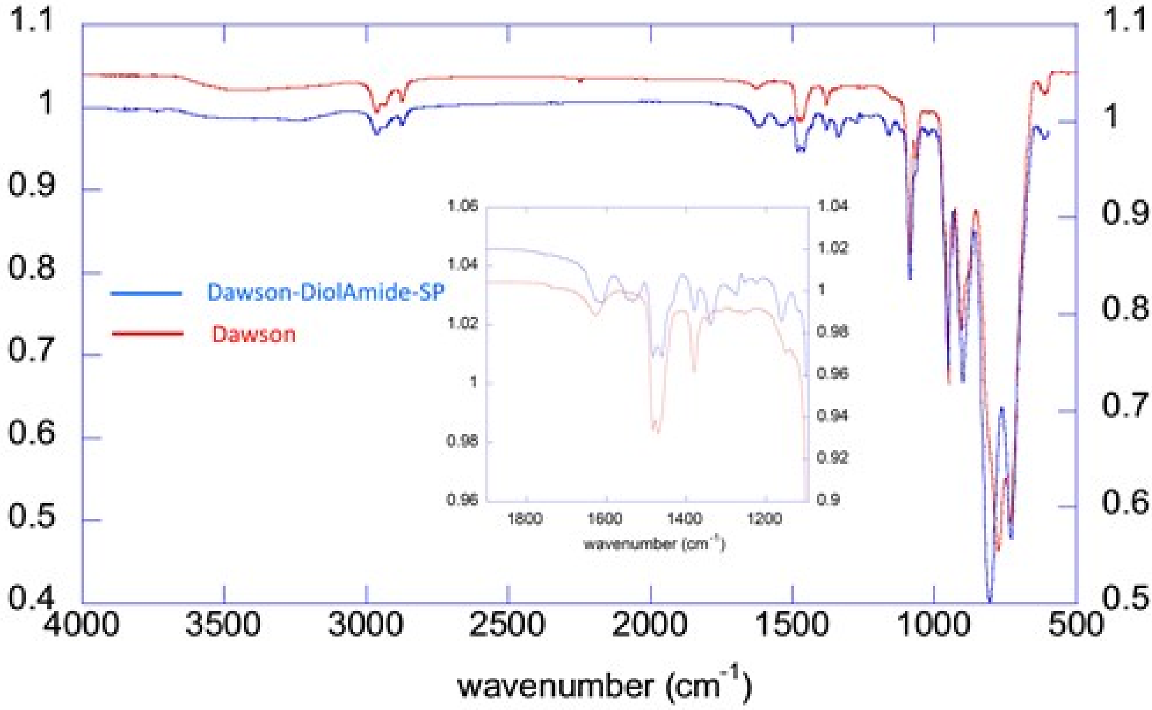

Figure S24 IR spectra of $(TBA)_5[H_4P_2W_{15}V_3O_{62}]$ and $\mathbf{(TBA)_5[P_2W_{15}V_3\text{-}SP]}$

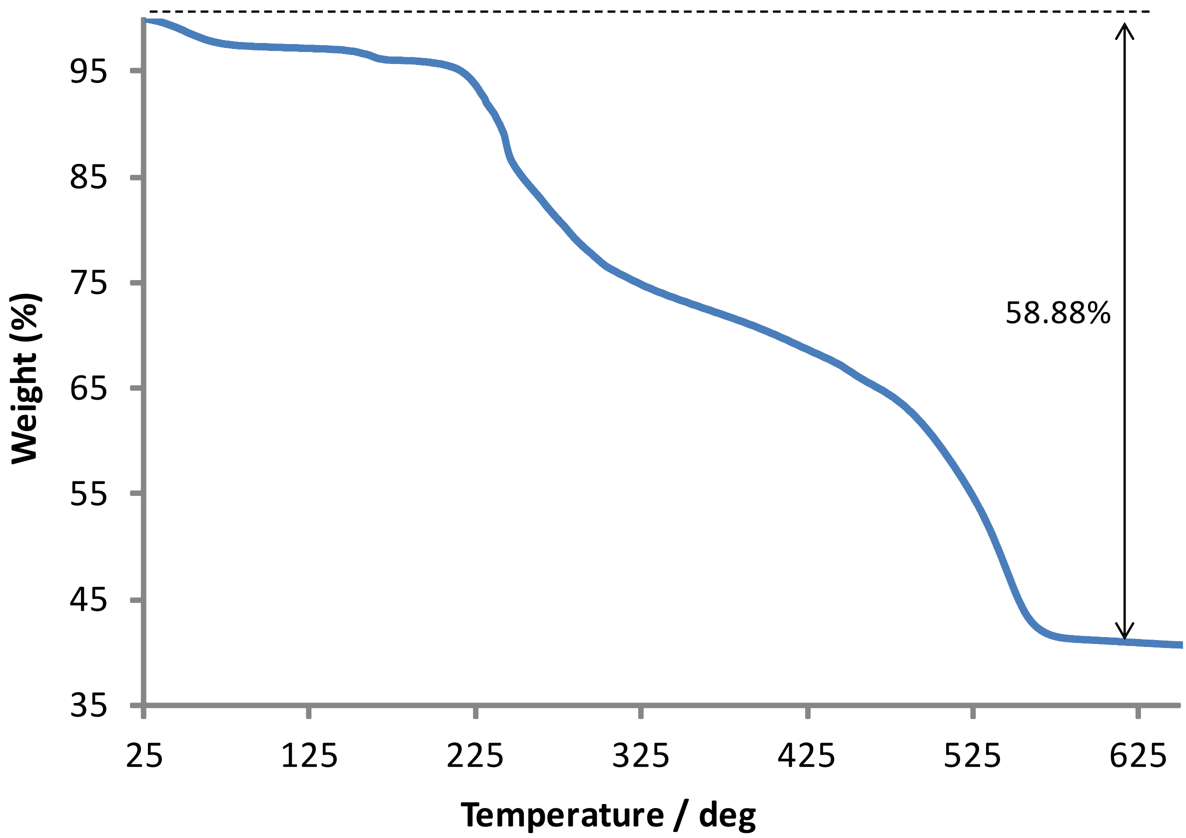

Figure S25. TGA curve of **$(TBA)_3[AlMo_6SP]$** (the calculated weight loss value considering oxides formation is 58.15 %wt)

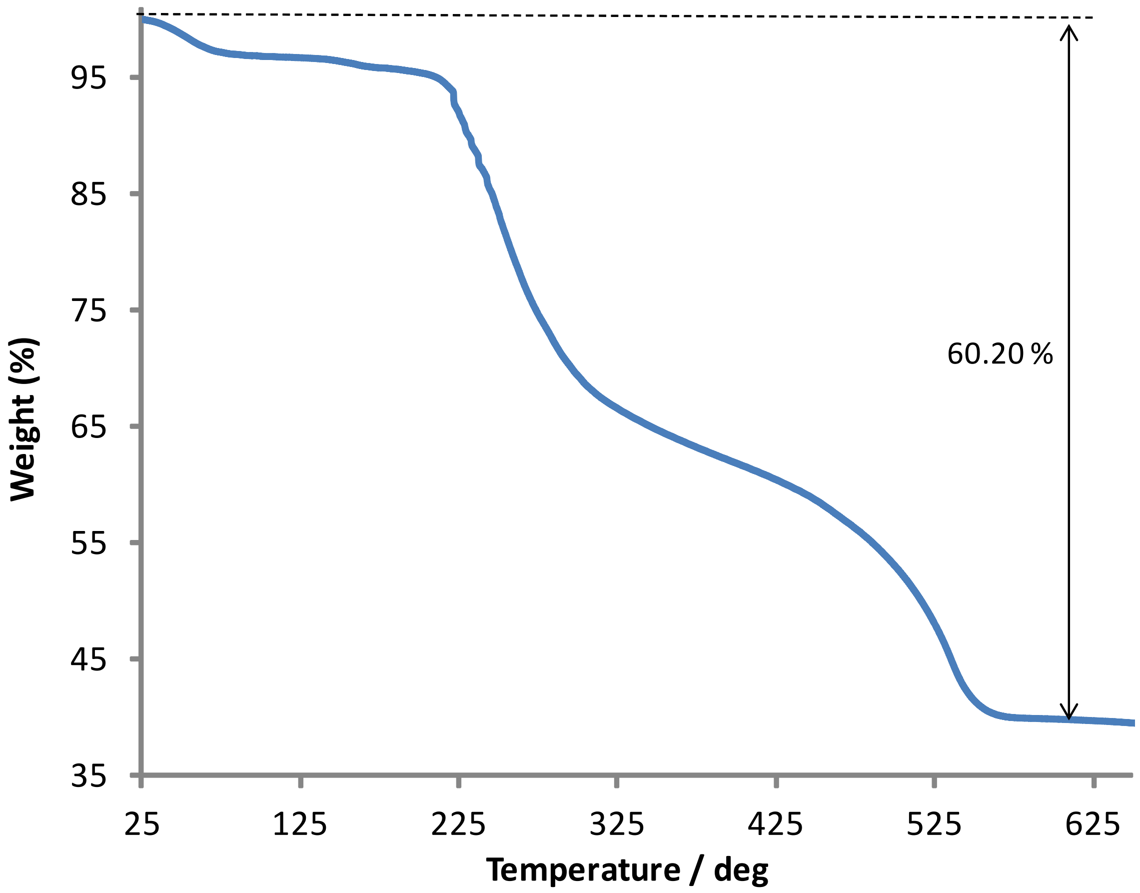

Figure S26. TGA curve of **$(TBA)_3[AlMo_6SN]$** (the calculated weight loss value considering oxides formation is 58.95 %wt)

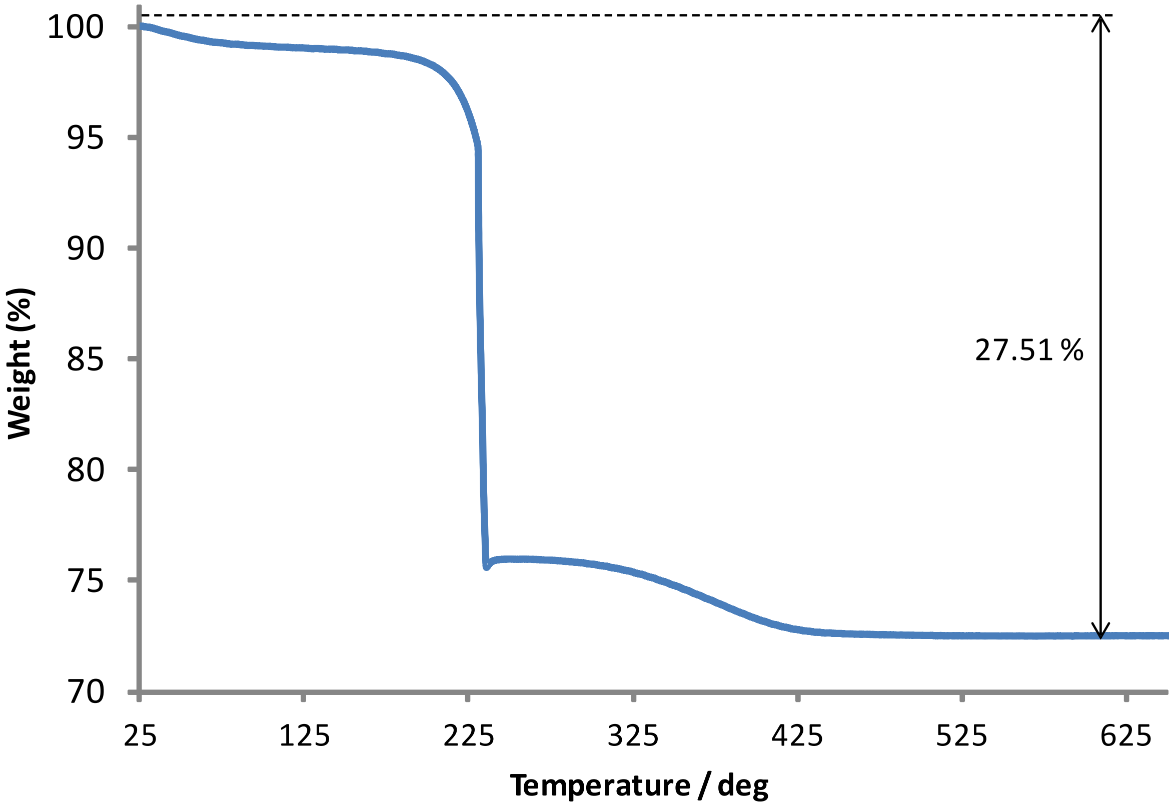

Figure S27. TGA curve of **(TBA)$_5$[P$_2$W$_{15}$V$_3$-SP]** (the calculated weight loss value considering oxides formation is 26.51 %wt)

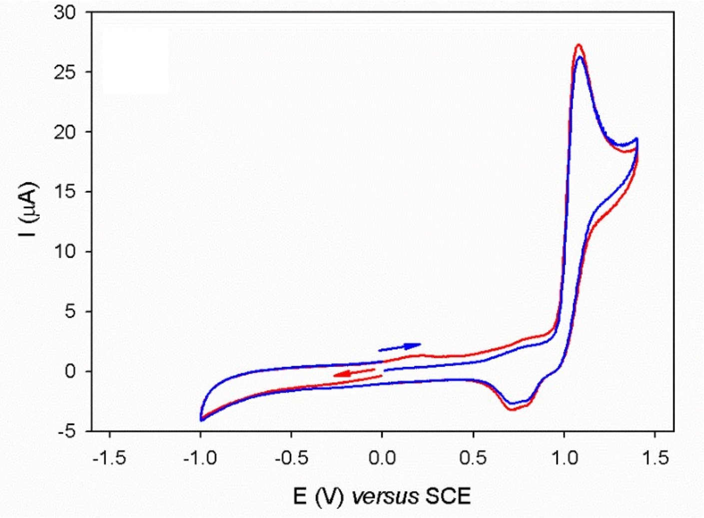

Figure S28. Cyclic voltammograms of **SP(OH)$_2$** (c = 1 mM) at a glassy carbon electrode (d = 3 mm) *vs.* SCE in CH_3CN with 0.1 M TBAPF$_6$ as the supporting electrolyte. Scan rate: 100 mVs^{-1}.

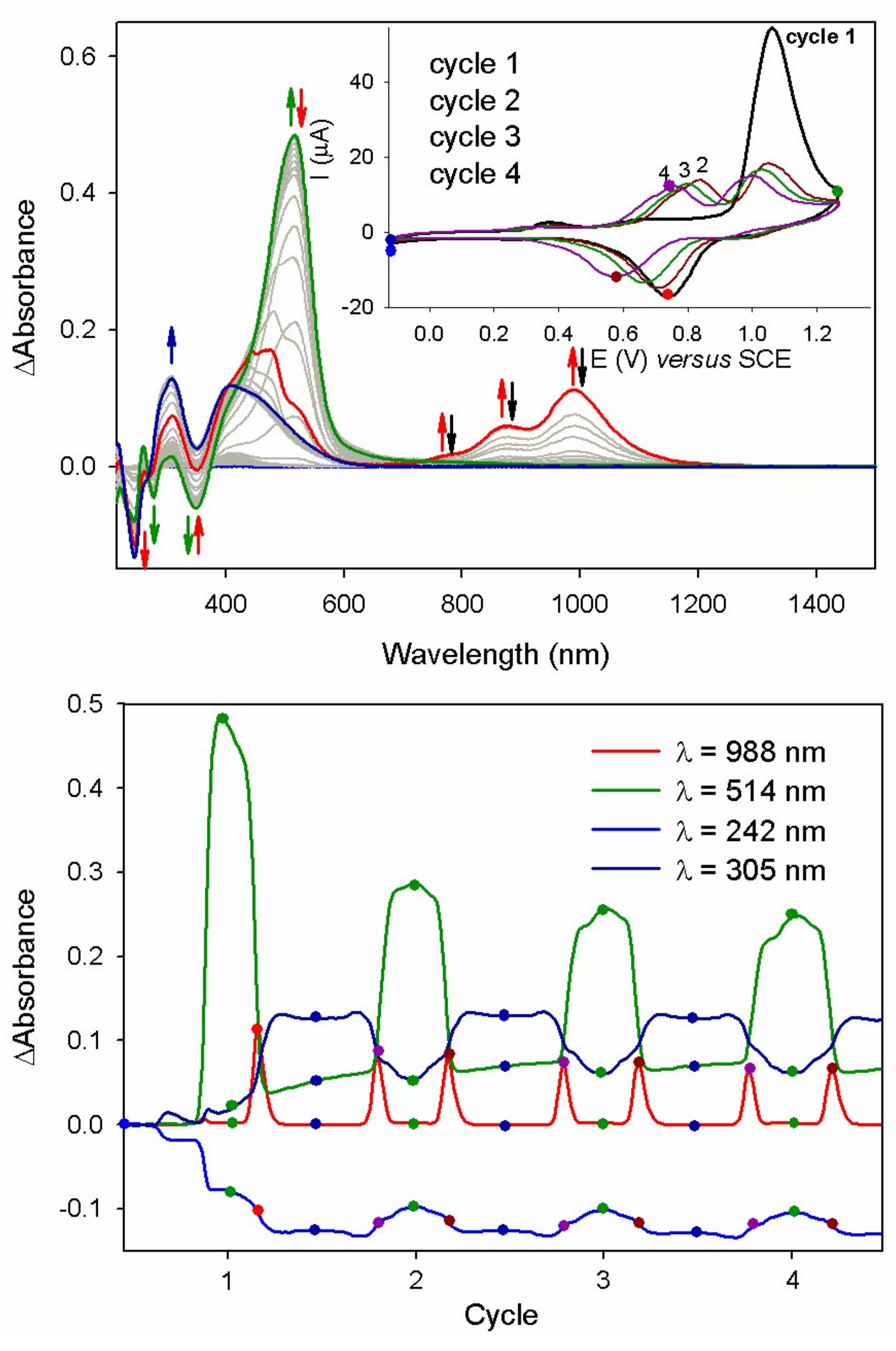

Figure S29. Differential UV-Vis-NIR spectroelectrochemical study of **SP(OH)$_2$** (c = 1 mM) at ambient temperature upon electrochemical oxidation in CH_3CN with 0.1 M $TBAPF_6$ as the supporting electrolyte recorded with an optically transparent thin-layer (0.2 mm) electrochemical (OTTLE) cell equipped with an Au minigrid WE and CaF_2 optical windows. A) UV-Vis-NIR spectra recorded during the four successive oxidations of the **SP(OH)$_2$** (between 0 and +1.4 V). Inset shows the corresponding CV at scan rate of 0.02 V.s^{-1}. B) Evolution of the intensity of absorption of the differential UV-vis-NIR spectra of **SP(OH)$_2$** at 988 nm, 514 nm, 305 nm and 242 nm over four switching cycles upon electrochemical reduction in the potential region of the oxidation step.

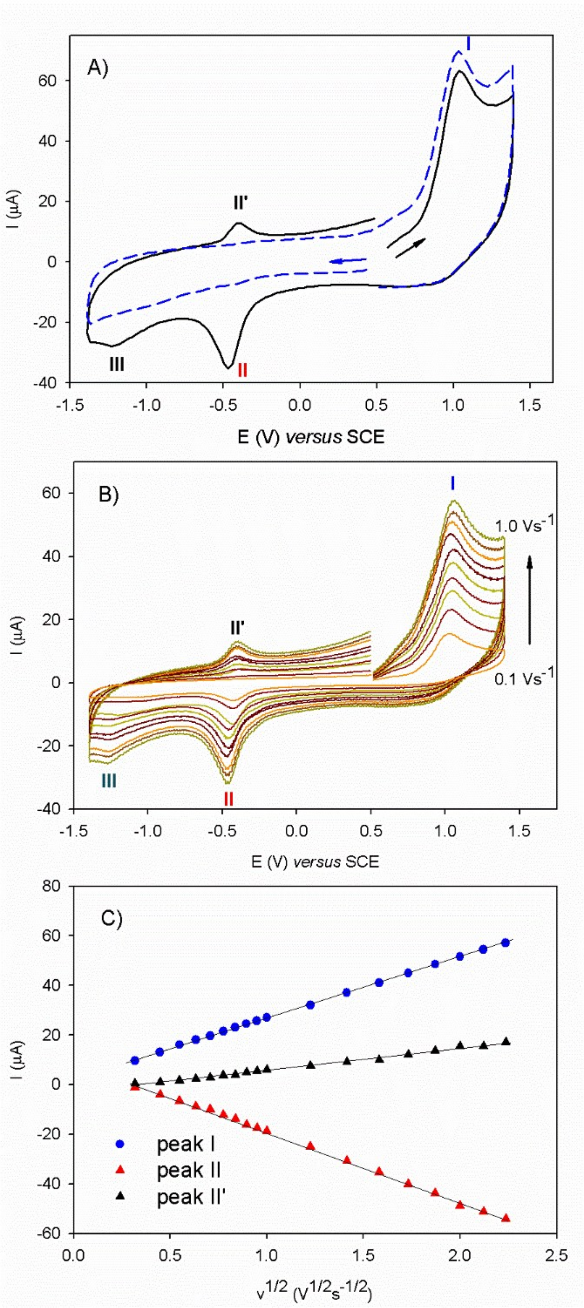

Figure S30. A) Cyclic voltammograms of **$(TBA)_3[AlMo_6$-SN]** (c = 1 mM) at a glassy carbon electrode (d = 3 mm) *vs.* SCE in CH_3CN with 0.1 M $TBAPF_6$ as the supporting electrolyte. Scan rate: 100 mVs^{-1}. B) cyclic voltammograms at different scan rates from 0.100 to 1.000 Vs^{-1}.C) plots of I_{pc} *vs.* $v^{1/2}$ for peaks I, II and II'.

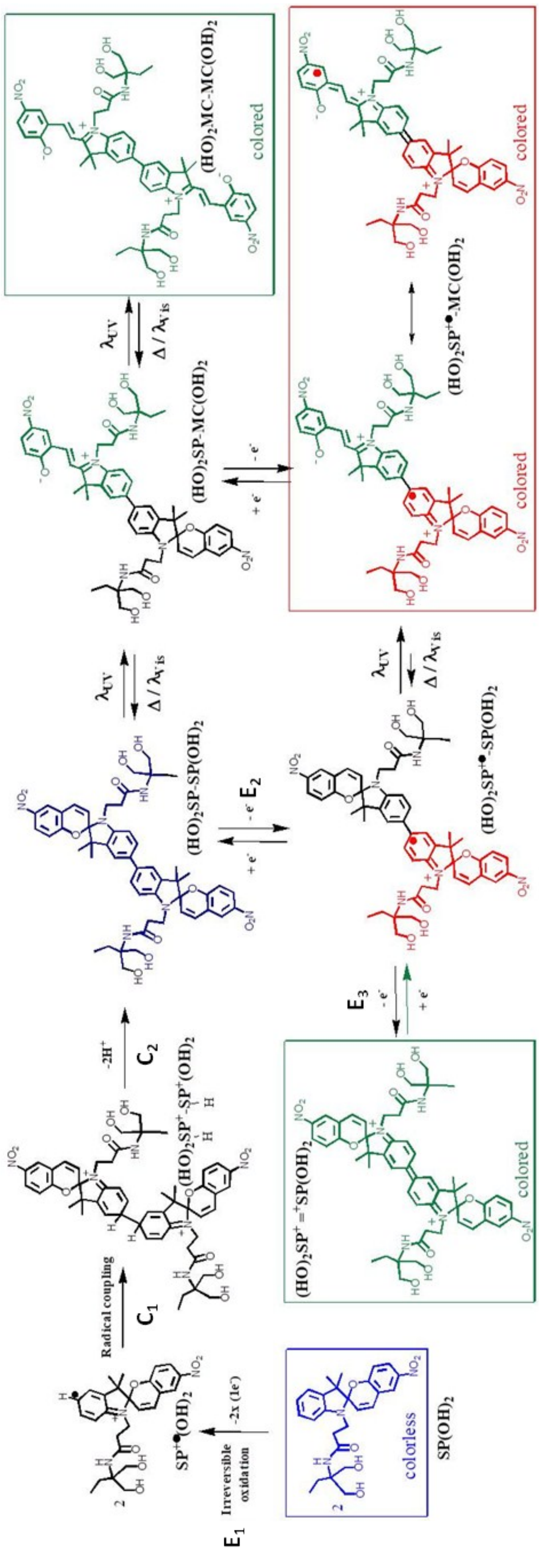

Scheme S1. Proposed mechanism explaining the spectroelectrochemical properties of **SP(OH)$_2$** (E$_1$, C$_1$, C$_2$, E$_2$ and E$_3$ refer to electrochemical and chemical reaction steps occuring during the oxidation of spiropyran, see text and ref 39 for details) .

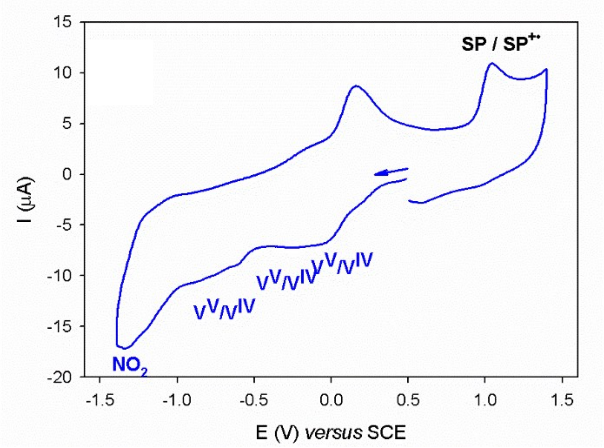

Figure S31. Cyclic voltammograms of **(TBA)$_5$[P$_2$W$_{15}$V$_3$-SP]** (c = 1 mM) at a glassy carbon electrode (d = 3 mm) *vs.* SCE in CH$_3$CN with 0.1 M TBAPF$_6$ as the supporting electrolyte. Scan rate: 100 mVs^{-1}.

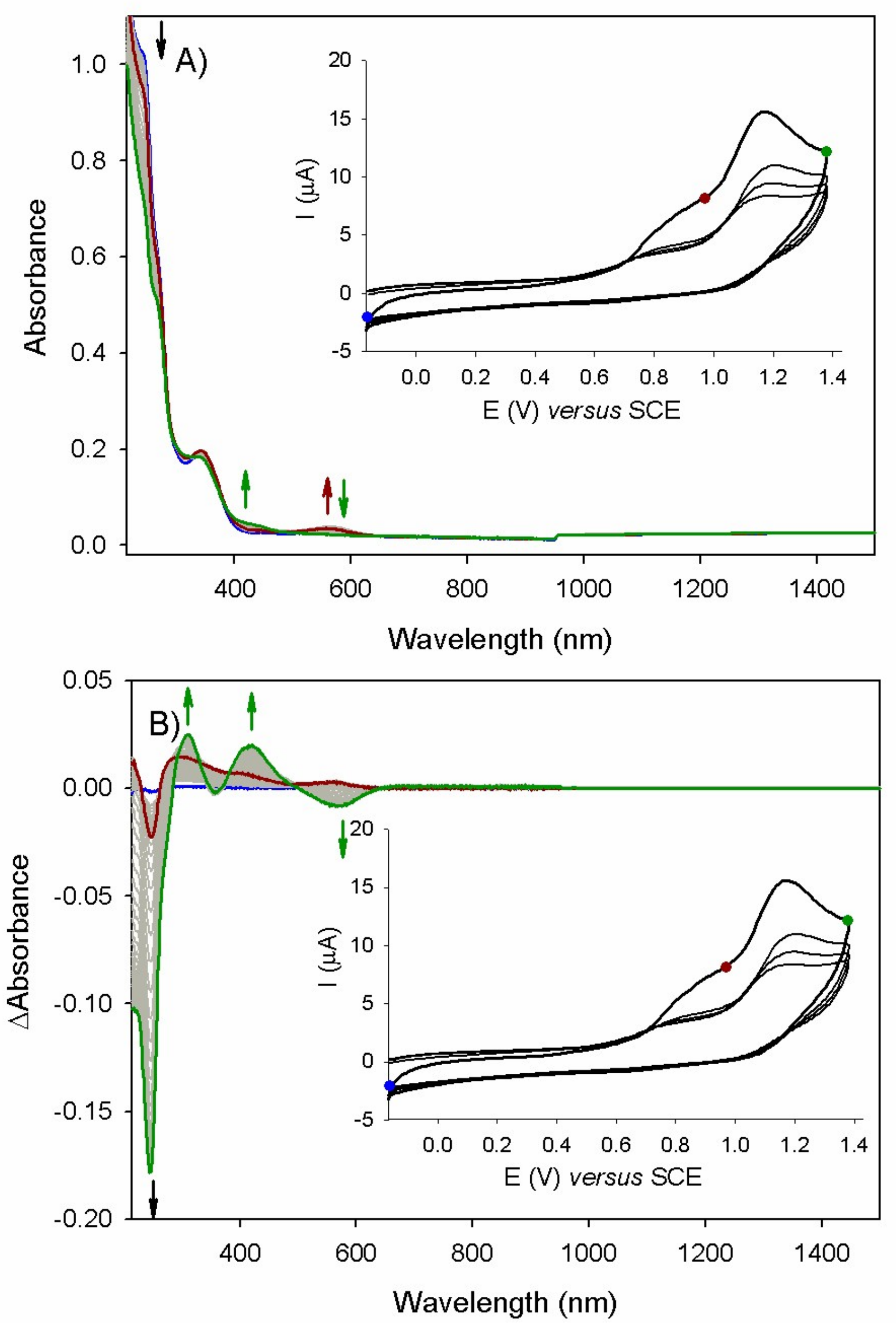

Figure S32. A) UV-Vis-NIR spectroelectrochemical and B) differential UV-Vis-NIR spectroelectrochemical study of **(TBA)$_3$[AlMo$_6$-SP]** (c = 1 mM) at ambient temperature upon electrochemical oxidation in CH_3CN with 0.1 M $TBAPF_6$ as the supporting electrolyte recorded with an optically transparent thin-layer (0.2 mm) electrochemical (OTTLE) cell equipped with an Pt minigrid WE and CaF_2 optical windows. Inset shows the corresponding CV at scan rate of 0.02 V.s^{-1}.

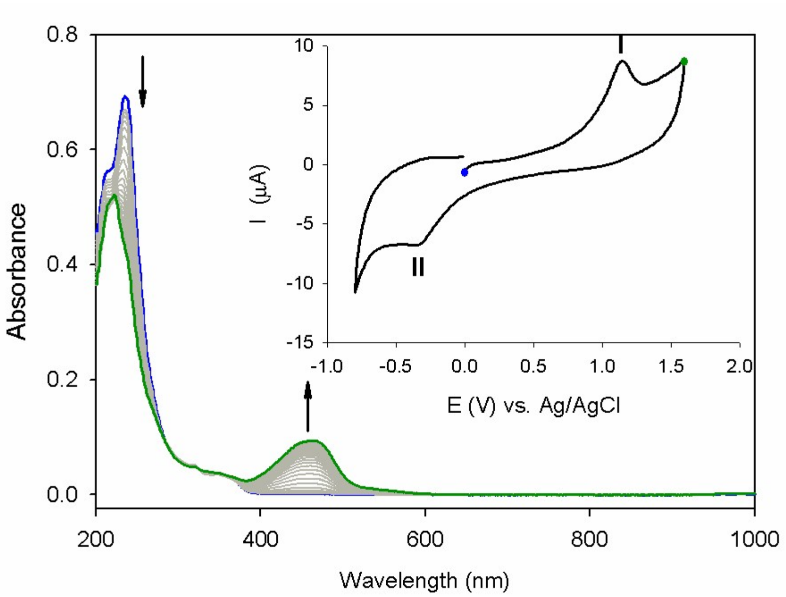

Figure S33. UV-Vis-NIR spectroelectrochemical study of **(TBA)$_3$[AlMo$_6$-SN]** (c = 1 mM) at ambient temperature upon electrochemical oxidation in CH_3CN with 0.1 M $TBAPF_6$ as the supporting electrolyte recorded with an optically transparent thin-layer (0.2 mm) electrochemical (OTTLE) cell equipped with an Au minigrid WE and CaF_2 optical windows. Inset shows the corresponding CV at scan rate of 0.02 V.s^{-1}.

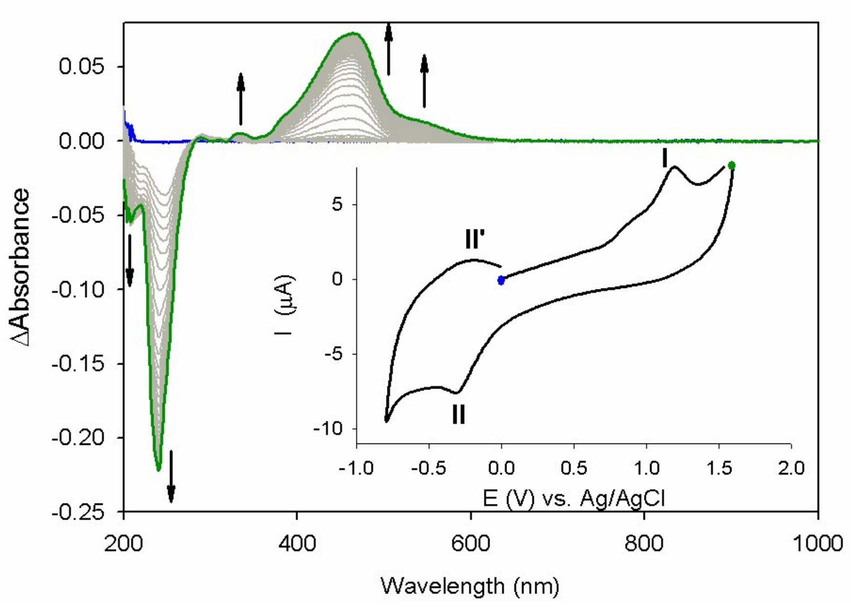

Figure S34. Differential UV-Vis-NIR spectroelectrochemical study of **(TBA)$_3$[AlMo$_6$-SN]** (c = 1 mM) at ambient temperature upon electrochemical oxidation in CH_3CN with 0.1 M $TBAPF_6$ as the supporting electrolyte recorded with an optically transparent thin-layer (0.2 mm) electrochemical (OTTLE) cell equipped with an Au minigrid WE and CaF_2 optical windows. Inset shows the corresponding CV at scan rate of 0.02 V.s^{-1}.

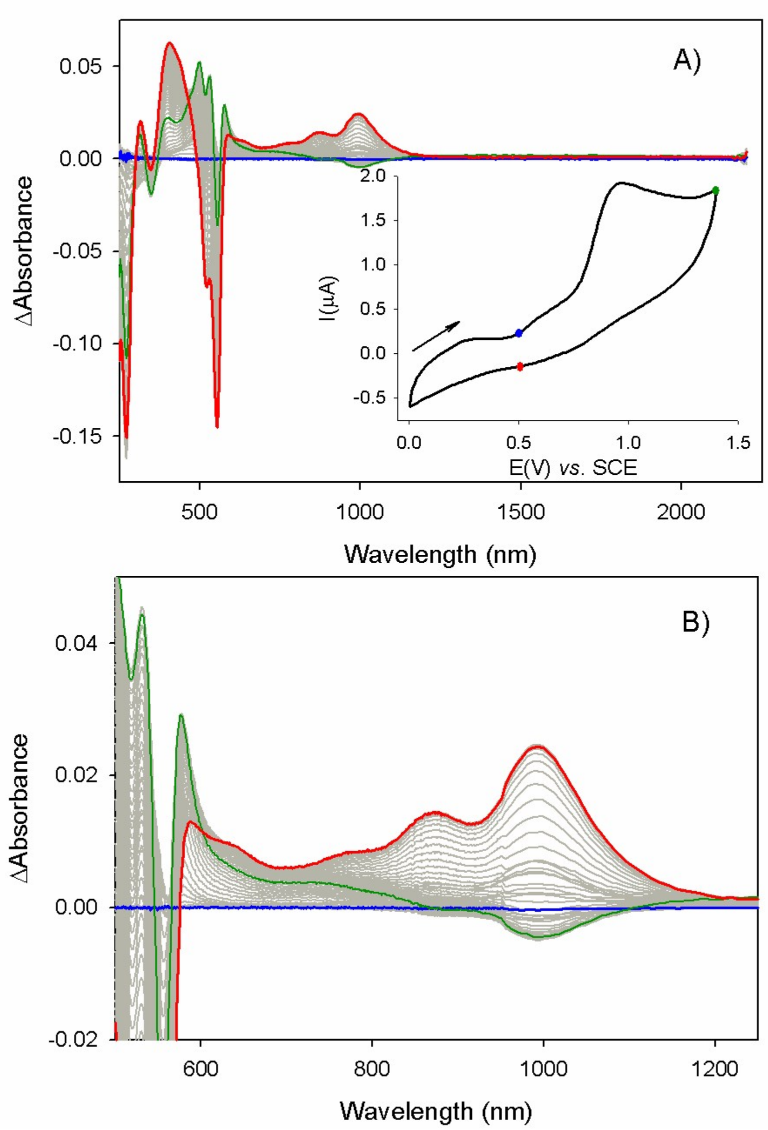

Figure S35. A) and B) Differential UV-Vis-NIR spectroelectrochemical study of **(TBA)$_5$[P$_2$W$_{15}$V$_3$-SP]** (c = 1 mM) at ambient temperature upon electrochemical oxidation in CH_3CN with 0.1 M $TBAPF_6$ as the supporting electrolyte recorded with an optically transparent thin-layer (0.2 mm) electrochemical (OTTLE) cell equipped with an Au minigrid WE and CaF_2 optical windows. Inset shows the corresponding CV at scan rate of 0.02 V.s^{-1}.

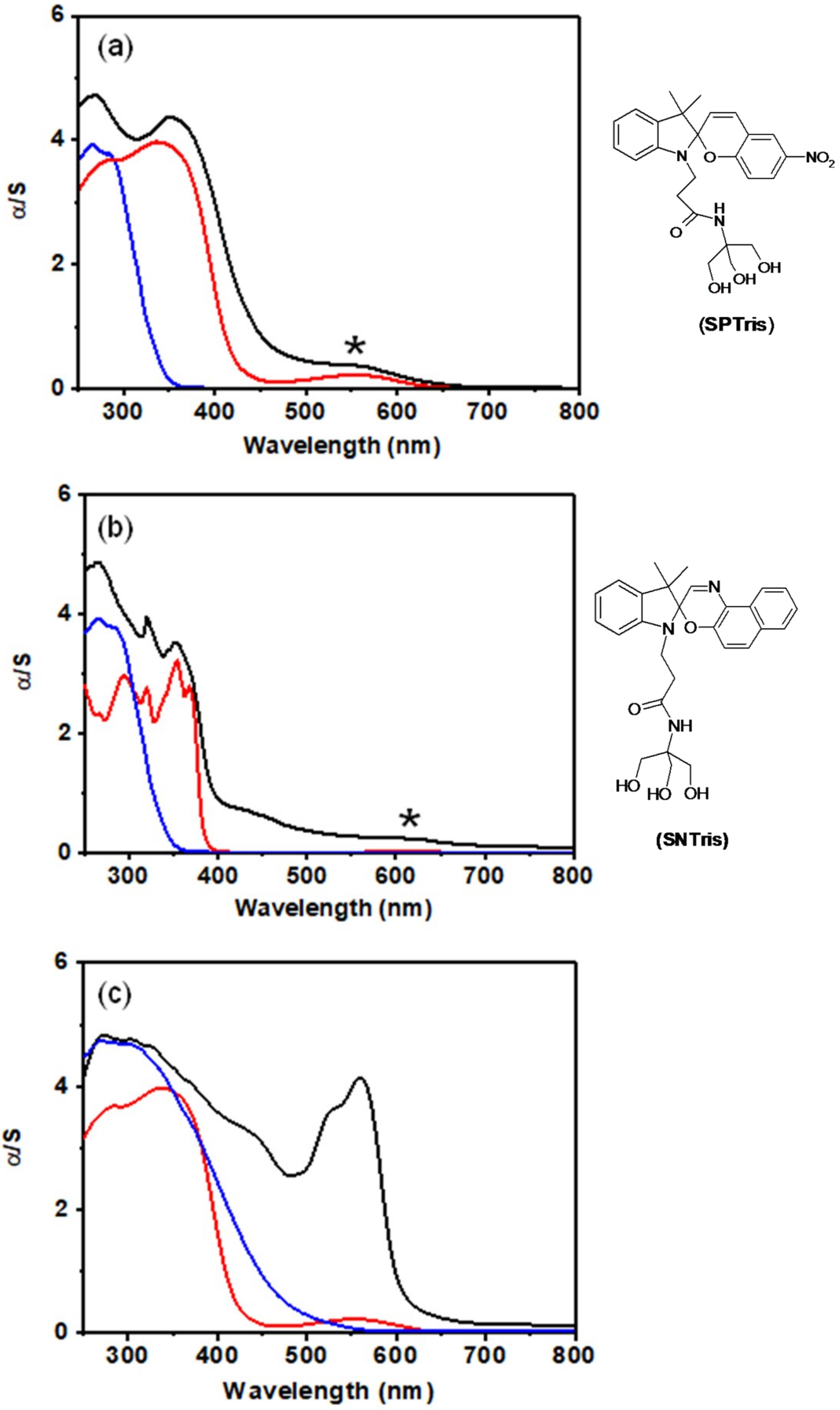

Figure S36. Kubelka-Munk transformed reflectivity *vs* wavelength of (a) **$(TBA)_3[AlMo_6$-SP]** (black line), **SPTris** (red line), and $(TBA)_3[AlMo_6(OH)_3\{(OCH_2)_3CNH_2\}]$ (blue line), (b) **$(TBA)_3[AlMo_6$-SN]** (black line), **SNTris** (red line), and $(TBA)_3[AlMo_6(OH)_3\{(OCH_2)_3CNH_2\}]$ (blue line) and (c) **$(TBA)_5[P_2W_{15}V_3$-SP]** (black line), **SPTris** (red line), and $(TBA)_5[H_4P_2W_{15}V_3O_{62}]$ (blue line). The weak absorptions in the visible in the spectra of **$(TBA)_3[AlMo_6$-SP]**, **$(TBA)_3[AlMo_6$-SN]** and **SPTris** (as indicated by the asterisks) are assignable to a small amount of the open "merocyanine" form which is responsible for the slight color of the powdered samples.

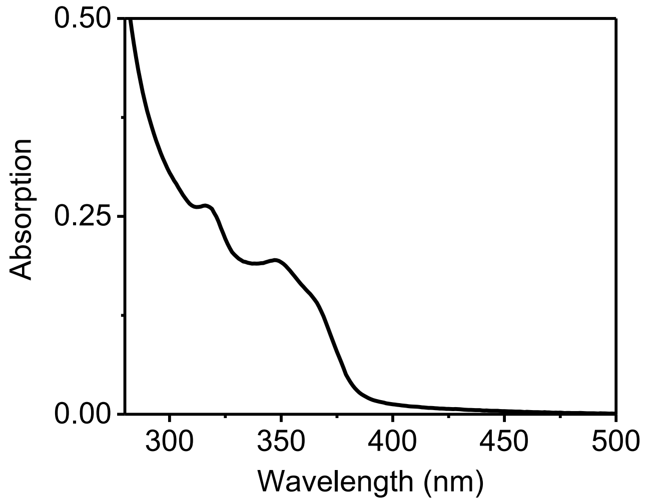

Figure S37. UV-vis absorption spectrum in acetonitrile (4.6×10^{-5} mol/L) of **$(TBA)_3[AlMo_6\text{-}SN]$**.

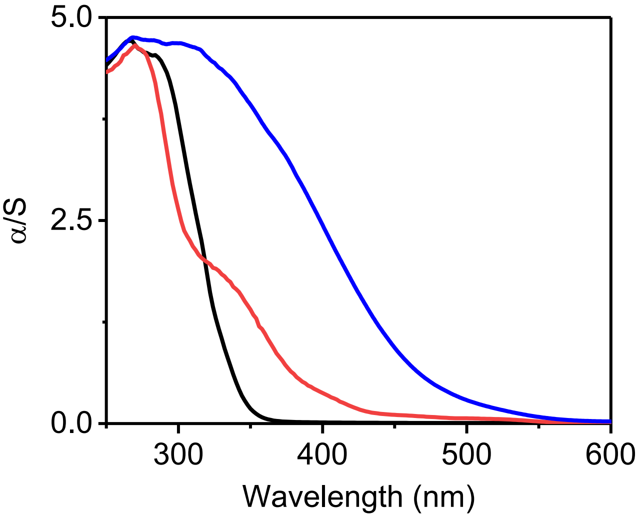

Figure S38. Kubelka-Munk transformed reflectivity *vs* wavelength of $(TBA)_3[AlMo_6(OH)_3\{(OCH_2)_3CNH_2\}]$ (black line), $(TBA)_3[MnMo_6O_{18}\{(OCH_2)_3CNH_2\}_2]$ (red line) and $(TBA)_5[H_4P_2W_{15}V_3O_{62}]$ (blue line).

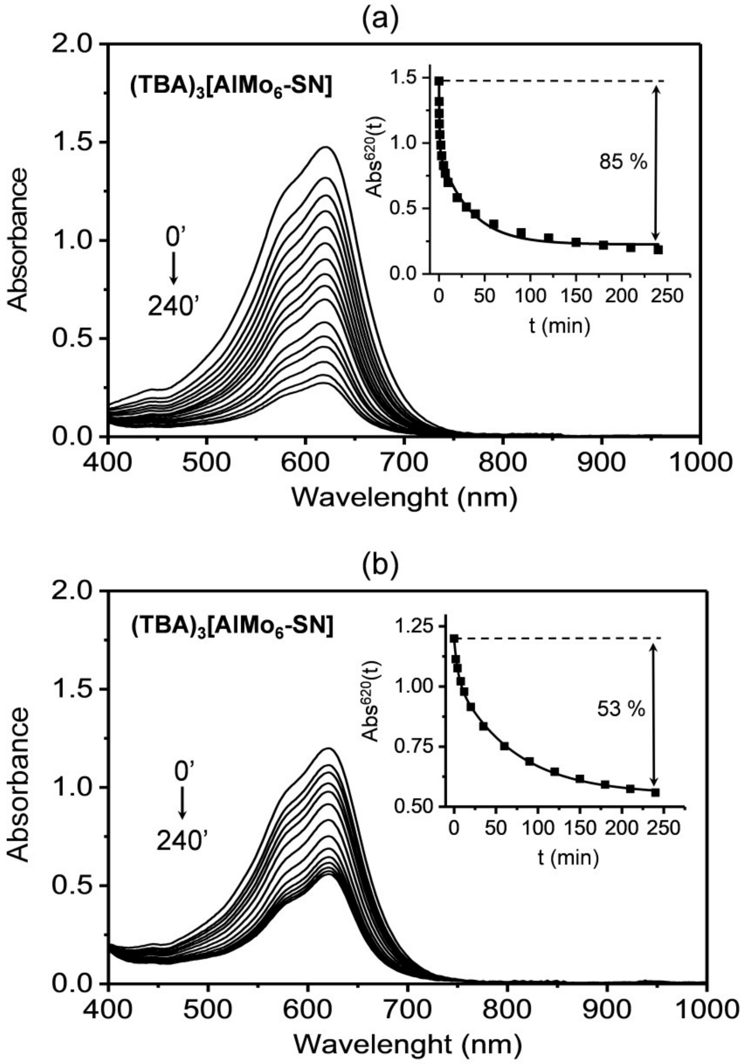

Fig. S39. Evolution of the photogenerated absorption at room temperature for **$(TBA)_3[AlMo_6$-SN]** (a) under visible light (λ_{irr} = 630 nm) after 0, 0.166, 0.333, 0.5, 1, 2, 3, 5, 7, 10, 20, 30, 40, 60, 90 and 120 min, and (b) in the dark during the thermal fading after 0, 2, 4, 8, 12, 20, 35, 60, 90, 120, 150, 180, 210 and 240 min. Insets: Temporal evolutions of $Abs^{620}(t)$. Black lines show the fits of the $Abs^{620}(t)$ *vs t* plots according to the rate law $Abs^{620}(t) = (A_0-A_1-A_2) + A_1\exp(-k^f_1t) + A_2\exp(-k^f_2t)$. Percents of absorption loss after 4 hours are also indicated.

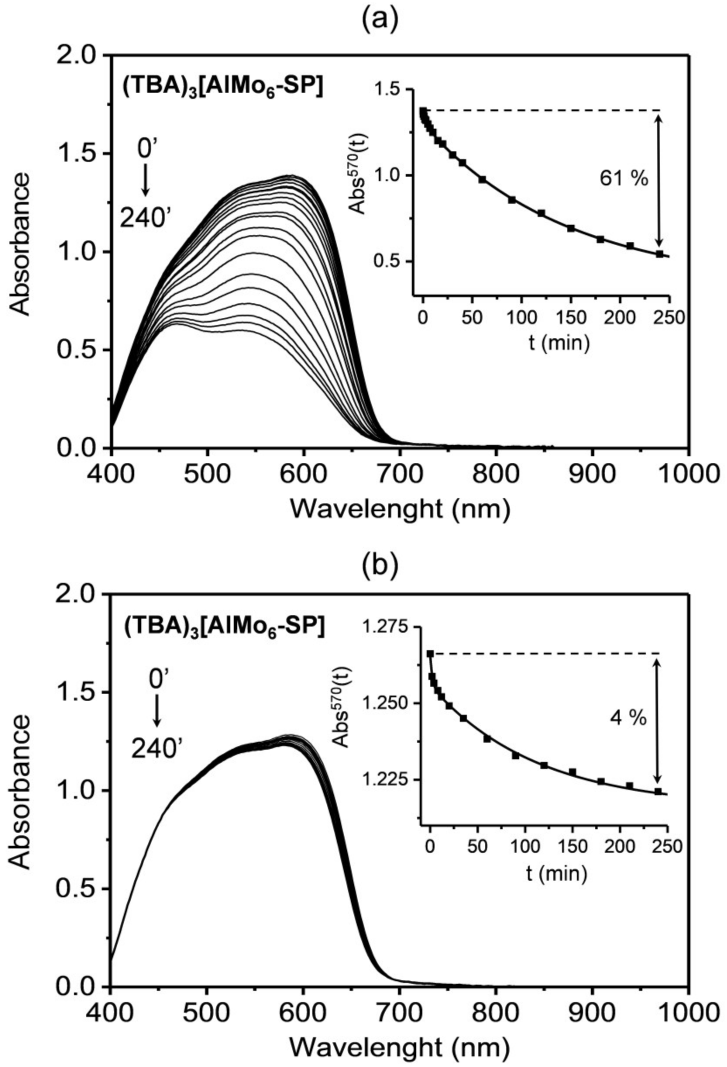

Fig. S40. Evolution of the photogenerated absorption at room temperature for **(TBA)$_3$[AlMo$_6$-SP]** (a) under visible light (λ_{irr} = 590 nm) after 0, 0.166, 0.333, 0.5, 1, 2, 3, 5, 7, 10, 15, 20, 30, 40, 60, 90, 120, 150, 180, 210, and 240 min, and (b) in the dark during the thermal fading after 0, 2, 4, 8, 12, 20, 35, 60, 90, 120, 150, 180, 210 and 240 min. Inset: Temporal evolutions of Abs^{570}(*t*). Black lines show the fits of the Abs^{570}(*t*) *vs t* plots according to the rate law $Abs^{570}(t) = (A_0\text{-}A_1\text{-}A_2) + A_1\exp(-k^f_1 t) + A_2\exp(-k^f_2 t)$. Percents of absorption loss after 4 hours are also indicated.

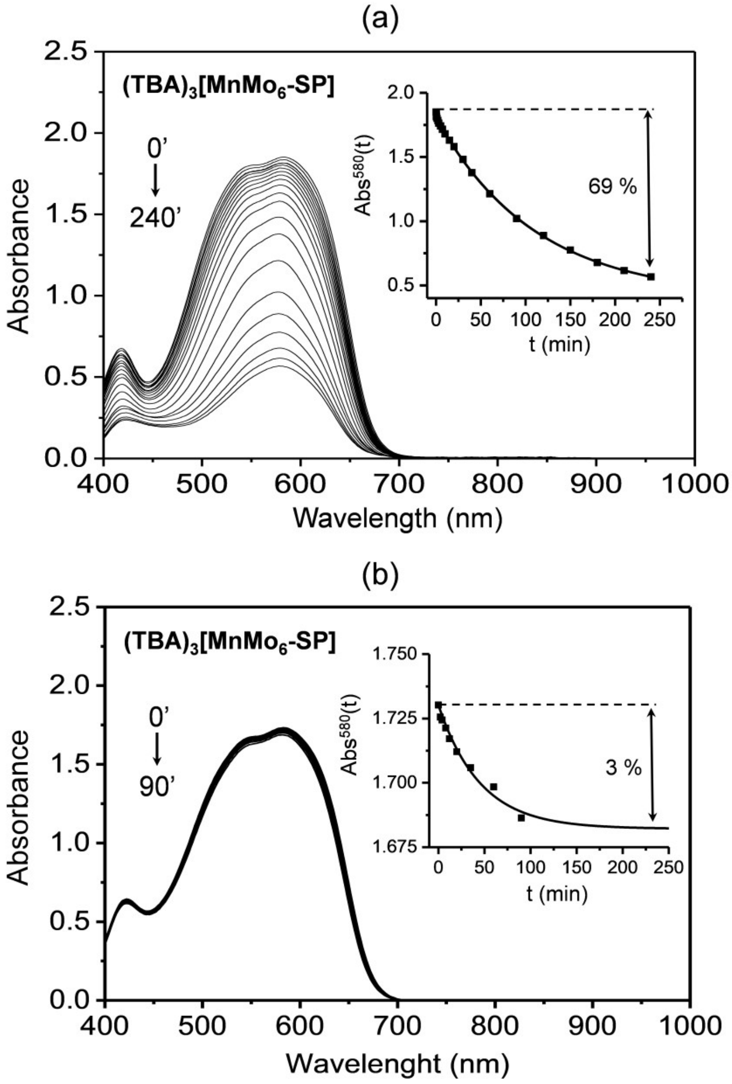

Fig. S41. Evolution of the photogenerated absorption at room temperature for **$(TBA)_3[MnMo_6\text{-}SP]$** (a) under visible light (λ_{irr} = 590 nm) after 0, 0.166, 0.333, 0.5, 1, 2, 3, 5, 7, 10, 15, 20, 30, 40, 60, 90, and 120 min, and (b) in the dark during the thermal fading after 0, 2, 4, 8, 12, 20, 35, 60, and 90 min. Inset: Temporal evolutions of $Abs^{580}(t)$. Black lines show the fits of the $Abs^{580}(t)$ *vs t* plots according to the rate law $Abs^{580}(t) = (A_0\text{-}A_1\text{-}A_2) + A_1\exp(-k^f_1 t) + A_2\exp(-k^f_2 t)$. Percents of absorption loss after 4 hours are also indicated.

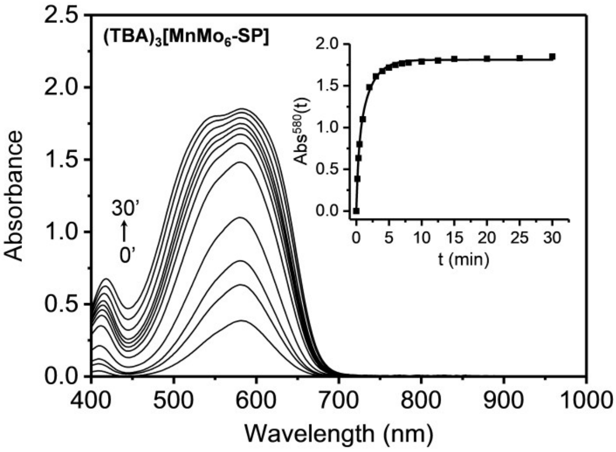

Fig. S42. Evolution of the photogenerated absorption at room temperature under UV irradiation (λ_{irr} = 365 nm) after 0, 0.166, 0.333, 0.5, 1, 2, 3, 4, 5, 6, 10, 20 and 30 min for **(TBA)$_3$[MnMo$_6$-SP]**. Inset: Temporal evolutions of Abs^{580}(*t*) under 365 nm-UV irradiation. The black line shows the fits of the Abs^{580}(*t*) *vs t* plots according to the rate law Abs^{580}(*t*) = ($A_1 + A_2$) - A_1exp(-$k^c{}_1$*t*) - A_2exp(-$k^c{}_2$*t*).

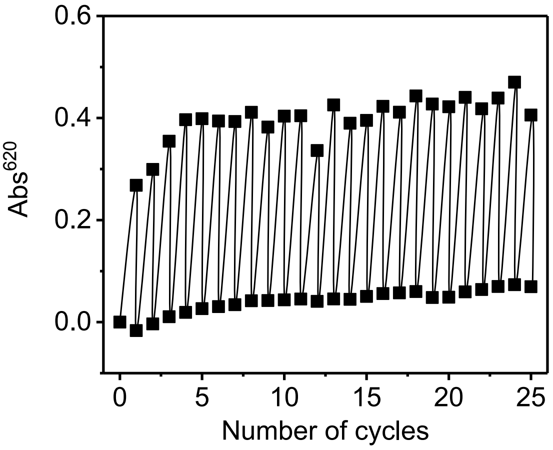

Figure S43. Evolution of the maximum of the photogenerated absorption at λ_{max} = 620 nm for **(TBA)$_3$[AlMo$_6$-SN]** during successive coloration/bleach cycles at room temperature. For one cycle, the sample is exposed to UV light (365 nm) for 20 s, and to red light (630 nm) for 4 min (the black lines display the mean values of the absorption in the coloured and bleached states). After a short period of activation, the hybrid system shows a good cyclability.

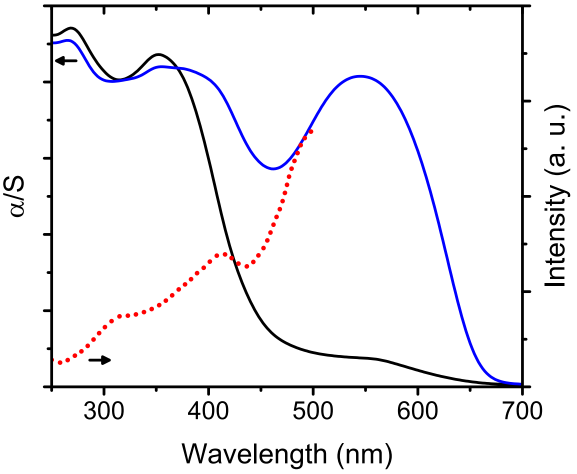

Figure S44. Kubelka-Munk transformed reflectivity *vs* wavelength spectra of **(TBA)$_3$[AlMo$_6$-SP]** before (black solid line) and after 20 min of 365-nm UV irradiation (blue solid line), and photoluminescence excitation (PLE) spectrum of **(TBA)$_3$[AlMo$_6$-SP]** monitored at λ_{em} = 675 nm (red dotted line).

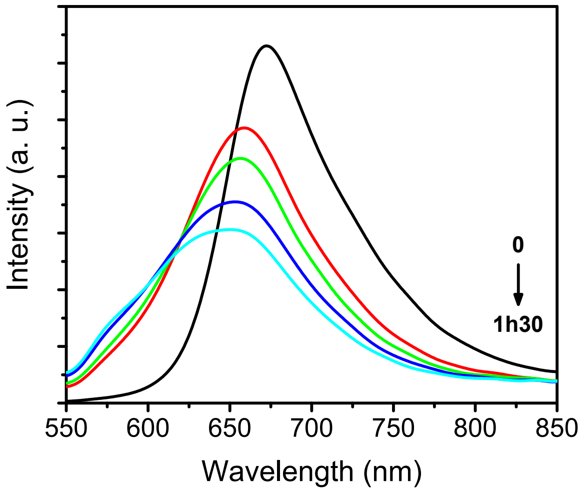

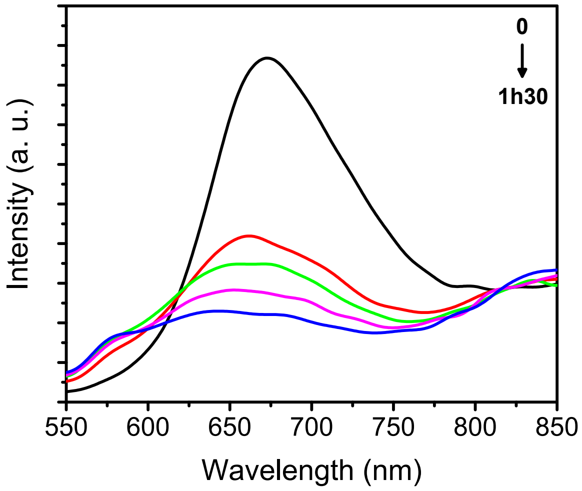

Figure S45: Evolutions of the merocyanine luminescence (monitored at λ_{exc} = 500 nm) under visible-light irradiation range (λ_{irr} = 590 nm) after 15, 30, 45, and 90 min for **(TBA)$_3$[AlMo$_6$-SP]** (top) and **(TBA)$_3$[MnMo$_6$-SP]** (bottom).